Komatiites: their geochemistry and origins

Pedro Waterton[a] and Nicholas Arndt[b]

a) University of Copenhagen, Department of Geosciences and Natural Resource Management. Øster Voldgade 10, 1350 København K. pw@ign.ku.dk
b) Institut des Sciences de la Terre, University Grenoble Alpes, CS 40700, 38058 GRENOBLE Cedex 9, France.

***This preprint is a book section that has been accepted for publication. Please reference as:

Waterton, P. & Arndt, N. Komatiites: their geochemistry and origins. In: Homann, M. et al. (eds) *The Archaean Earth: Tempos and Events (2nd Edition of The Precambrian Earth).* Elsevier.***

Abstract

Komatiites are ultra-hot ultramafic lavas, largely restricted to the Archaean. They represent an extreme endmember of terrestrial magmatism and challenge our understanding of how mantle melting operates. We briefly introduce this compositionally diverse group of lavas and critically evaluate constraints on their formation. Despite evidence for moderate water contents in some komatiites, the vast majority require an unusually hot mantle source and probably formed by critical melting in dry or 'damp' plumes. The low concentrations of incompatible trace elements in most komatiites cannot be explained by residual phases rich in these elements and instead reflect high degrees of partial melting. Constraining the melting pressures of komatiites is complicated by a lack of robust constraints. However, high MgO contents, high degrees of partial melting, and evidence of residual garnet in the formation of Al-depleted komatiites indicate that melting began at considerable depth in the upper mantle, if not within the lower mantle. We combine these constraints to present models for komatiite formation. Al-depleted komatiites are high pressure melts of fertile mantle; they segregated from sources containing residual garnet at pressures >7 GPa and possibly >10 GPa. Al-undepleted komatiites segregated at lower pressures and/or after reaching higher degrees of partial melting. They came from a depleted source that may have formed by low degrees of hydrous melting in the mantle transition zone. Al-enriched, or Ti-depleted komatiites originated from extremely depleted sources. Their melting pressures are difficult to ascertain, but evidence from the Commondale komatiites suggest at least some formed at pressures >10 GPa. Ti-enriched komatiites and post-Archaean komatiites were produced by smaller degrees of melting of variably enriched or depleted sources, with melting conditions comparable to those of modern picrites.

1 Introduction

1.1 Why the interest?

When Wilson (2019) described olivine in the 3.3 Ga Commondale komatiites with Fo contents up to 96.6, he built a case that these were Earth's hottest lavas. Using olivine-melt Mg-Fe exchange, he calculated that the MgO content of the melt was a remarkably high 36.1 wt%, corresponding to a liquidus temperature of 1670°C. This is 450C° hotter than modern basalts.

Komatiites are the hottest lavas on Earth and an extreme example of partial melting in the Earth's mantle. Their high temperatures influenced how they erupted and crystallized, raise intriguing questions about komatiite mantle sources, and allow komatiites to act as a geological thermometer tracing the hottest parts of the Earth's mantle.

Despite decades of interest, numerous questions surround the formation of komatiites and what they tell us about the mantle's thermal and compositional history. Although the existence of ultramafic magmas has been widely accepted ever since the discovery of komatiites (Viljoen and Viljoen, 1969; Nesbitt, 1971; Pyke *et al.*, 1973; Green *et al.*, 1975), debate has persisted about how they were generated, leading to a proliferation of formation models (e.g., Shimizu *et al.*, 2001; Parman *et al.*, 2004; Bédard, 2006; Serrano *et al.*, 2011; Robin-Popieul *et al.*, 2012; Herzberg, 2016; Sobolev *et al.*, 2016; Sossi *et al.*, 2016; McKenzie, 2020; Wyman, 2020). Komatiite occurrences are highly heterogeneous in both space and time (Condie and O'Neill, 2010), leading to questions about the thermal structure and temporal evolution of the Earth's mantle (Nisbet *et al.*, 1993; Trela *et al.*, 2017). Komatiites are increasingly used to trace the secular evolution of mantle chemistry (Campbell and Griffin, 1992; Maier *et al.*, 2009; Amsellem *et al.*, 2019; Nicklas *et al.*, 2019; Puchtel *et al.*, 2022), though the implications of using the compositions of magmas as diverse as komatiites for this purpose are just beginning to be explored (Waterton *et al.*, 2021).

The main petrological and geochemical characteristics of komatiites, their field characteristics, and mode of eruption have been covered in several books and numerous papers, and will not be repeated in detail here. Instead, following a brief description of the rock type, we focus on the major advances in our understanding of the origin of komatiites made in the past two decades.

1.2 Komatiite definitions and flow morphologies

Komatiites were first recognised as ultramafic lavas by Viljoen and Viljoen (1969), who named them after the Komati River, which runs through the type-locality in the Barberton greenstone belt, South Africa. The first generally agreed upon definition (Arndt and Brooks, 1980), recognised komatiite as a rock type, the ultramafic equivalent (>18 wt% MgO) of basalt. More recent definitions describe komatiites as ultramafic rocks with textures or geological context indicating a volcanic origin (Kerr and Arndt, 2001; Arndt *et al.*, 2008), <1 wt% TiO_2 (Le Bas, 2000; Hanski *et al.*, 2001), and <52 wt% SiO_2 (Pearce and Reagan, 2019). Some definitions require that komatiites are derived from liquids with >18 wt% MgO. These criteria distinguish komatiites from other volcanic rocks, including: picrites, which may have >18 wt% MgO due accumulation of olivine in more evolved liquids (Francis, 1985; Hole and Natland, 2020); meimechites, high-TiO_2 alkaline ultramafic lavas formed by low degree, high pressure hydrous melting (Arndt *et al.*, 1995; Ivanov *et al.*, 2018); and boninites, high SiO_2 ultramafic magmas formed by flux melting of highly depleted sources, usually in subduction settings (Cameron *et al.*, 1979). It is important to note that all known komatiites are metamorphosed or altered to some degree, though the prefix meta-komatiite is rarely used.

Komatiites display a variety of flow morphologies (Barnes, 2006; Arndt *et al.*, 2008). Best known are differentiated lava flows (**Figure 1**), which are differentiated into a spinifex-textured upper part and an olivine cumulate lower part. Spinifex texture comprises centimetre- to metre-sized skeletal plates of olivine (Nesbitt, 1971) or pyroxene (Lowrey *et al.*, 2017), or needles of pyroxene (Viljoen and Viljoen, 1969), arranged perpendicular to flow margins (platy spinifex) or randomly oriented (random spinifex). These skeletal crystals are surrounded by a matrix of finer-grained olivine, clinopyroxene and altered glass (Pyke *et al.*, 1973; **Figure 2a**).

Not all komatiite flows are structured in this manner and the majority totally lack spinifex texture (Hill *et al.*, 1995; Dann, 2000). Some komatiite flows are porphyritic throughout, containing variable amounts of mm-sized equant olivine phenocrysts in a matrix of fine-grained pyroxene and altered glass; others are composed largely or entirely of ortho- to adcumulates. More rarely, komatiites occur as pillow lavas (Pyke *et al.*, 1973; Dann, 2000), or fragmental komatiites of hyaloclastic or pyroclastic origin (Arndt *et al.*, 1977; Gélinas *et al.*, 1977; Echeverría and Aitken, 1986; Révillon *et al.*, 2000).

Flow thicknesses range from <50 cm to >100 m (Hill *et al.*, 1995; Barnes and Lesher, 2008). Their lengths are difficult to define due to limited exposure, but some individual flows are continuous for 100s of metres and komatiite-dominated sequences can be traced for 100s of kilometres (Hill *et al.*, 1995; Ayer *et al.*, 2002).

1.2.1 Spinifex texture

Spinifex textures are best developed in smaller flows, on the flanks of large eruptions, or in lava lakes. This indicates that low flow rates or lava ponding are prerequisites for their formation (Arndt, 1986; Hill *et al.*, 1995; Puchtel *et al.*, 1996; Barnes, 2006). Thicknesses of spinifex zones can vary, or the texture can disappear altogether, within single flows (Arndt *et al.*, 1977). Spinifex usually grows downwards from the top of komatiite flows. The lowest portion of the spinifex zone therefore has the most evolved compositions and, along with the top of the cumulate layer, is the last part of the flow to crystallise (Pyke *et al.*, 1973; Arndt *et al.*, 1977; Renner *et al.*, 1994). Platy spinifex zones may contain a cumulus component of excess olivine or pyroxene (Campbell and Arndt, 1982; Arndt, 1986); their bulk-rock compositions shouldn't be used as a proxy for komatiitic melts (Nisbet *et al.*, 1993).

The origin of spinifex texture has long been debated (Viljoen and Viljoen, 1969; Nesbitt, 1971). Central to this debate is the so-called 'spinifex paradox': skeletal spinifex grains resemble crystals grown during rapid cooling, yet these crystals are found well below the flow top, where cooling rates are low (Donaldson, 1982). A resolution to this paradox was proposed by Faure *et al.* (2006), who demonstrated experimentally that platy spinifex textures form within thermal gradients in the upper parts of komatiite flows. Growth of olivine (or pyroxene) from the flow top forms a zone of melt depleted in olivine; crystallisation within this zone results in skeletal morphologies. Crystals are orientated perpendicular to the flow top because only vertically orientated crystals can grow without colliding with other crystals (Turner *et al.*, 1986; Shore and Fowler, 1999). Cooling rates as low as 2 °C per hour can produce platy spinifex textures, providing thermal gradients are present, whereas random olivine spinifex forms at faster cooling rates nearer the flow tops (Faure *et al.*, 2006).

The reason why spinifex textures are absent in most komatiites and similar ultramafic lavas, such as Phanerozoic picrites, remains unresolved despite numerous discussions (Pyke *et al.*, 1973; Turner *et al.*, 1986; Barnes and Lesher, 2008). In major komatiite flow channels, high flow rates or turbulent flow (Barnes and

Lesher, 2008) may prevent the establishment of the thermal gradients or solidification of an upper flow crust required for spinifex growth. More generally, spinifex can only form in the absence of phenocrysts, which act as nuclei for crystal growth, suppressing the formation of skeletal habits (Lofgren, 1983). Spinifex formation may therefore require upstream deposition of phenocrysts (Barnes and Lesher, 2008), or deposition of cumulate layers when sufficiently low viscosity lavas slow or pond (Pyke *et al.*, 1973), to allow formation of a crystal-free upper layers. Superheating during magmatic ascent could also achieve a similar effect by clearing the melt of crystal nuclei (Aitken and Echeverría, 1984; Arndt, 1994). Picrites or komatiites that do not produce a crystal-free layer upon ponding, either because the carrier melts are too viscous or the degree of crystallinity is too high (Marsh, 1981), may be unable to form spinifex textures.

1.2.2 When is spinifex not spinifex?

Two other textures in ultramafic rocks can be mistaken for spinifex and may be used to mistakenly identify komatiites (**Figure 2b, c**). The first is 'microspinifex' texture. While this term is correctly used for zones of fine-grained randomly oriented skeletal crystals of olivine or pyroxene in the upper parts of some komatiite flows, it is not appropriate for the dendritic pyroxenes found interstitial to olivine phenocrysts in many picrites. This type of texture is found in olivine-phyric rocks with diverse origins and is not diagnostic of komatiite (Cameron and Nisbet, 1982; Arndt *et al.*, 2008). A simple criterion is that the term spinifex should be reserved for textures visible in hand samples and avoided for textures observed only in thin section.

The second texture consists of radiating bladed or lenticular olivine grains, up to 1 m long, in dunites that have undergone high-grade metamorphism (Collerson *et al.*, 1976). These olivines can be distinguished from 'true' spinifex by the non-skeletal morphology of olivine grains, an elongation along the olivine b-axis (rather than a or c for magmatic spinifex), and association with secondary hydrous minerals that are commonly cross-cut by the olivine blades (Evans and Trommsdorff, 1974; Snoke and Calk, 1978).

1.2.3 Komatiitic and tholeiitic basalts

Komatiitic basalts are mafic volcanic rocks that contain olivine or pyroxene spinifex textures (Arndt, 1982; Lowrey *et al.*, 2017), or are genetically related to komatiites (Nesbitt *et al.*, 1982). In some areas a genetic association is evident because the rocks are interlayered with komatiite lava flows or form the mafic portions of layered mafic-ultramafic flows (Arndt *et al.*, 1977). However, elsewhere genetic associations are harder to identify and a relationship to komatiites must be established through geochemical or isotopic data. The bulk-rock compositions of some komatiitic basalts may exceed 18 wt% MgO due to olivine accumulation, but these should not be classed as komatiites if it can be shown that their parental magmas had <18 wt% MgO (Hanski and Smolkin, 1995; Puchtel *et al.*, 1996; Wilson and Riganti, 2022).

Tholeiitic basalts are the most common rock type associated with komatiites and the major constituent of most Archaean and Proterozoic greenstone belts. There is an ongoing debate over the relationship between these basalts and komatiites; whether they formed by differentiation of komatiitic parental melts or by independent melting of similar mantle sources (Arndt and Nesbitt, 1982; Campbell *et al.*, 1989; Waterton *et al.*, 2020), but this issue is not addressed further here.

2 Spatial and temporal distribution of komatiites

Komatiites are unevenly distributed in both space and time. They are primarily an Archaean phenomenon

(Nesbitt *et al.*, 1982; Nisbet, 1982) and komatiite abundances decreased sharply after 2.7 Ga (**Figure 3**). Only a few komatiite localities are known from the Proterozoic, including those in the ~1.9 Ga Circum-Superior belt (Arndt, 1982; Waterton *et al.*, 2017) and Baltic Shield (Puchtel *et al.*, 1997; Hanski *et al.*, 2001). There are no known komatiites from the period between 1.8 and 0.8 Ga. The only well-documented Phanerozoic example are the Cretaceous Gorgona komatiites (Echeverria, 1980); Permian Song-Da komatiites (Hanski *et al.*, 2004) lack macrospinifex texture and are arguably picrites (Anh *et al.*, 2011). Even within the Archaean, komatiite occurrences are highly heterogeneous. The oldest known komatiites are the ~3.53 Ga Coonterunah komatiites or ~3.55 Ga Schapenburg komatiites (Van Kranendonk *et al.*, 2007; Maier *et al.*, 2009; Puchtel *et al.*, 2016). No convincing examples of Eoarchaean komatiites have been documented.

Komatiites also have a strongly uneven spatial distribution. Archaean komatiites are generally restricted to low-grade granite-greenstone terranes and are absent from high-grade metamorphic terranes, though this may be something of a tautology as it is doubtful that volcanic textures, including spinifex, would survive granulite-facies metamorphism (Nutman *et al.*, 1996). Some high-grade metamorphosed ultramafic rocks have been claimed to be komatiites on the basis of geochemistry (Kalsbeek and Manatschal, 1999; Frank *et al.*, 2016), but these have low MgO compared to most komatiites.

More broadly, komatiite abundances vary strongly between different Archaean cratons. Some, such as the Yilgarn and Superior Cratons, are home to abundant komatiites (Nesbitt *et al.*, 1979; Hollings *et al.*, 1999; Thurston *et al.*, 2008; Mole *et al.*, 2014), while the Slave and North Atlantic Cratons entirely lack komatiite. The reasons for this uneven spatial distribution remain unclear. Haphazard preservation is almost certainly a factor, supported by the presence of komatiitic chromite in detrital quartzites from Slave and Kaapvaal Cratons, which demonstrates that some komatiites were lost to erosion (Haugaard *et al.*, 2021; Lowe *et al.*, 2021). Varying erosional depths may also contribute; some deeply eroded cratons that lack komatiite lavas contain abundant intrusive peridotite or dunite bodies, which probably represent komatiitic cumulates (Chadwick and Crewe, 1986; Rollinson *et al.*, 2002; Szilas *et al.*, 2018). Finally, evidence that komatiite eruption is strongly localised along crustal boundaries or rifts suggests lithospheric controls on komatiite eruption (Mole *et al.*, 2014, 2021). Early stabilisation of thick lithosphere (Pearson *et al.*, 1995; Timmerman *et al.*, 2022) may have therefore impeded komatiite formation or eruption, either locally or at the craton scale.

3 Geochemistry and types of komatiite

Komatiites show a wide range of compositions. Early studies distinguished three main types, primarily on the basis of Al_2O_3/TiO_2 and heavy rare-earth element (HREE) patterns (**Figure 4**; Nesbitt *et al.*, 1979; Jahn *et al.*, 1982). Al-depleted (Barberton-type) komatiites have low Al_2O_3/TiO_2 and high Gd/Yb; Al-undepleted (Munro-type) komatiites have near-chondritic ratios of the two parameters; and Al-enriched komatiites have high Al_2O_3/TiO_2 and low Gd/Yb. The latter have also been referred to as 'Ti-depleted', because TiO_2 depletion exerts the main control on Al_2O_3/TiO_2 (Sproule *et al.*, 2002; Kamber and Tomlinson, 2019). Later, Ti-enriched (Karasjok type) komatiites were recognised (Barnes and Often, 1990). These are typically lower in MgO and have low Al_2O_3/TiO_2, though this arises from Ti-enrichment, rather than Al-depletion. Al-undepleted and Al-enriched komatiites tend to be relatively depleted in more incompatible trace elements, such as the light rare-earth elements (LREE; i.e., La/Sm ratios are low); Al-depleted and some, but not all, Ti-enriched komatiites show elevated La/Sm (**Figures 4, 5**).

Ti-enriched and Al-depleted komatiites are not easily distinguished using element and oxide ratios alone.

Though alternative classifications have been proposed, these either do not identify Al-enriched komatiites (Hanski *et al.*, 2001), or require knowledge of the parental melt composition (Sossi *et al.*, 2016). We therefore propose a classification scheme using the absolute Al_2O_3 and TiO_2 contents normalised to a common MgO content to correct for fractional crystallisation or accumulation of olivine (**Figures 4a, b**). We use 25% MgO because it is close the modal MgO value in Archean komatiites (Barnes and Arndt, 2019; Kamber and Tomlinson, 2019); element concentrations are normalised to this value by interpolating along regressions of Al_2O_3 and TiO_2 against MgO. We adopt the Al_2O_3/TiO_2 values suggested by Kamber and Tomlinson (2019) as boundaries between the groups: Al-depleted <15, Al-undepleted 15–25, Al-enriched >25, and suggest that komatiites with >0.5 wt% $(TiO_2)_{25}$ (where the subscript indicates the TiO_2 content estimated for a melt containing 25 wt% MgO) should be considered Ti-enriched.

This $(Al_2O_3)_{25}$ vs $(TiO_2)_{25}$ diagram documents the concentrations of Al_2O_3 and TiO_2, which are important parameters that are not recorded by element ratios alone. For example, the high Al_2O_3/TiO_2 of Commondale komatiites is mainly due to low TiO_2, whereas the low Al_2O_3/TiO_2 in Barberton Al-depleted komatiites reflects both moderately high TiO_2 and low Al_2O_3. Furthermore, the diagram shows that although all the Al-undepleted komatiites share near-chondritic Al_2O_3/TiO_2 (close to 20), they have very different concentrations of both elements, from very high in Gorgona komatiites, to strikingly low in Barberton Al-undepleted komatiites. The concentrations of Al are indicative of conditions at the site of melting, whereas $(TiO_2)_{25}$ reflects the degree of melting and prior melt extraction (**Section 4**). This approach should only be applied to suites where there is a tight correlation between the concentration of the element and MgO, indicative of control by a single olivine population. Scattered plots of Al_2O_3 and TiO_2 against MgO may indicate mixed phenocryst populations, as in some picrites, or mobility of these elements during metamorphism.

In addition to the $(Al_2O_3)_{25}$ vs $(TiO_2)_{25}$ diagram, we use two further plots to illustrate the geochemical compositions of komatiites (**Figures 4c, d**). 1) The Al_2O_3/TiO_2 vs $(Gd/Yb)_N$ diagram ('N' indicates normalisation to primitive mantle of Hofmann, 1988) initially proposed by Jahn *et al.* (1982), distinguishes the three main types of komatiite: Al-depleted, Al-undepleted and Al-enriched and shows the effect of garnet fractionation during their petrogenesis. 2) The $(La/Sm)_N$ vs $(Gd/Yb)_N$ diagram, which reflects the degree of LREE and HREE depletion or enrichment.

4 Constraints on komatiite formation

Most komatiite formation models have invoked the presence of mantle plumes, following the early recognition that (dry) ultramafic liquids have extremely high liquidus temperatures and, by extension, elevated mantle temperatures (Green, 1975; Green *et al.*, 1975). However, a wide range of alternatives have been proposed, either invoking the presence of water to lower the required temperatures, or invoking non-uniformitarian processes (**Figure 6**). Here we evaluate models of komatiite formation first by addressing questions relevant to the formation of all komatiites, before discussing models specific to the various komatiite types in **Section 5**.

4.1 Were komatiites, dry, wet or damp?

The amount of water in komatiite magmas has generated animated debate. Early studies proposed that the parent magmas formed by high-degree melting of their mantle source (Viljoen and Viljoen, 1969; Green *et al.*, 1975; Arndt, 1977; Nisbet, 1982). Given that water behaves as an incompatible element during mantle melting, and without *a priori* evidence for hydrous mantle sources, most authors assumed that komatiites

were essentially anhydrous. Nonetheless, 'wet' models invoking high water contents (> 1 wt%) appeared soon after. Key arguments for a hydrous origin include: an association with rocks interpreted to be arc volcanics, the hypothesis that water is required to form spinifex texture (Brooks and Hart, 1974; de Wit *et al.*, 1987), compositional similarities between komatiitic basalts and subduction zone magmas (Parman and Grove, 2005), and the compositions of certain komatiitic pyroxenes resemble those formed by water-saturated crystallisation (Parman *et al.*, 1997). In these models, komatiites represent a high temperature equivalent of boninites (Grove and Parman, 2004). More recently, Herzberg (2016) proposed that komatiites were generated in 'carbonated wetspots' – mantle sources with elevated concentrations of both CO_2 and H_2O, either in plumes or ambient mantle.

As noted previously, the formation of spinifex texture does not require the presence of water. Subduction-like geochemical signatures in some komatiites probably resulted from crustal contamination (Barnes and Arndt, 2019). Other arguments for a hydrous origin have been contested elsewhere (Arndt *et al.*, 1998, 2008). Two recent advances rule out high volatile contents in most komatiites. The first is the measurement of H_2O and CO_2 in melt inclusions in komatiitic olivine and spinel. These have consistently found low but significant H_2O contents between 0.2–1.0 wt% (Shimizu *et al.*, 2001; Sobolev *et al.*, 2016, 2019; Asafov *et al.*, 2018, 2020). Concentrations of CO_2 range from ~200 ppm in Archaean komatiites, to ~1700 ppm in Gorgona komatiites (Kamenetsky *et al.*, 2010; Gurenko *et al.*, 2016). The second advance is the advent of geothermometers that are independent of melt H_2O content, such as olivine-melt Sc/Y (Mallmann and O'Neill, 2013) and Al-in-olivine (Wan *et al.*, 2008; Coogan *et al.*, 2014). Where applied to komatiites, they give temperatures close to the anhydrous liquidus. These have been interpreted to indicate water contents from 0.1–0.6 wt% (Sobolev *et al.*, 2016; Waterton *et al.*, 2017), though these are somewhat poorly constrained due to large uncertainties in both the measured temperatures and the effect of water content on temperature (Herzberg, 2022).

Herzberg (2016) argued that melt inclusions studies may strongly underestimate H_2O contents, due to degassing prior to formation of the inclusions. However, degassing during a komatiite's ascent should trigger olivine crystallisation and trapping of melt inclusions, because the magma's liquidus temperature increases as the water content falls. Melt inclusions from boninites and meimechites support this reasoning, recording H_2O contents of up to 2.9 and 3.9 wt%, respectively (Sobolev and Chaussidon, 1996; Ivanov *et al.*, 2018); if komatiites had such high water contents, these should be observable.

We conclude that most komatiites contained <1 wt% H_2O. These water contents indicate mantle sources with a maximum of 0.5 wt% H_2O (Shimizu *et al.*, 2001), significantly higher than in the MORB source (Sobolev *et al.*, 2016), but not sufficiently hydrated to support models in which komatiites represent boninite-like flux melts (Parman *et al.*, 1997; Grove and Parman, 2004). Furthermore, CO_2 contents lower than typical MORB (Hauri *et al.*, 2018) are inconsistent with an origin from carbonated wetspots (Herzberg, 2016). The water in komatiites has been proposed to originate from the mantle transition zone (Shimizu *et al.*, 2001; Sobolev *et al.*, 2016, 2019; Asafov *et al.*, 2018, 2020), which may contain up to a few percent of water in wadsleyite and ringwoodite (Smyth, 1994; Pearson *et al.*, 2014).

Some komatiites probably had higher water contents, including igneous amphibole-bearing komatiites from the Abitibi belt (Stone *et al.*, 1997). Other komatiites may have picked up water via assimilation of hydrous material at a late stage during their ascent. Examples include the Murphy Well flow (Siégel *et al.*, 2014) and fragmental, arguably pyroclastic, komatiites from northern Sweden (Saverikko, 1985).

4.2 How hot were komatiites and their mantle sources?

4.2.1 Komatiite liquidus temperatures

Komatiite liquidus temperatures are most commonly estimated using the MgO content of the parental magma, which is proportional to the liquidus temperature for high MgO melts; a 1 wt% increase in MgO corresponds to around 20 °C increased liquidus temperature (Nisbet, 1982; Matzen *et al.*, 2011; Herzberg and Asimow, 2015). One approach to calculating parental melt MgO is to use a composition inferred to represent a komatiitic liquid, typically that of chilled margins or fine-grained random olivine spinifex. Though this method is straightforward, care needs to be taken because the margins of komatiite flows are susceptible to alteration, and even random olivine spinifex compositions can show evidence of MgO gain (Arndt, 1986). Furthermore, small quantities of olivine phenocrysts can have significant effects on the bulk rock MgO; 5 vol% of olivine phenocrysts will increase the MgO by ~1.5% (Waterton *et al.*, 2017), equivalent to a ~30 °C temperature overestimate. Parental melt compositions can also be calculated from olivine-melt Fe-Mg exchange (Roeder and Emslie, 1970; Toplis, 2005), either using measured olivine Mg#s, or by extrapolating olivine control lines in plots of incompatible elements to the MgO axis, to identify the average crystallising olivine composition (Bickle, 1982; Puchtel *et al.*, 2004). This process requires an estimate of the total Fe content of the parental magmas and, because only Fe^{2+} is incorporated into olivine, an estimate of $Fe^{2+}/\Sigma Fe$ (Berry *et al.*, 2008; Waterton *et al.*, 2017).

For komatiites, melt MgO contents and liquidus temperatures are typically calculated at atmospheric pressure, under the assumption that olivine only began to crystallise near the surface (e.g., Nisbet *et al.*, 1993; Puchtel *et al.*, 2013; Sobolev *et al.*, 2016; Sossi *et al.*, 2016). However, evidence that some komatiites begin crystallising olivine at great depth (Wilson and Bolhar, 2022) can cause incorrect estimates of the melt MgO content from olivine-melt Fe-Mg exchange, because the exchange coefficient is pressure dependent (Herzberg, 2022 and references therein). Ideally, several approaches to calculating parental melt MgO should be used (Bickle, 1982; Nisbet *et al.*, 1993; Herzberg *et al.*, 2007), before correcting the calculated dry liquidus temperatures for any water present (e.g., Sobolev *et al.*, 2016).

Liquidus temperatures calculated for common Archaean komatiites with ~23–30 wt% MgO range from ~1450–1600 °C (Nisbet *et al.*, 1993; Sossi *et al.*, 2016), or up to 1670 °C in rare komatiites with higher MgO contents (Robin-Popieul *et al.*, 2012; Wilson, 2019; Herzberg, 2022). The presence of small amounts of water in some Archaean komatiites lowered these by a maximum of 30–60 °C (Sobolev *et al.*, 2016; Asafov *et al.*, 2018), though the effect of water on liquidus temperatures could have been as small as 9–23 °C, depending on the calibration used (Herzberg, 2022). Proterozoic komatiites appear to have had lower MgO contents and liquidus temperatures; ~20–27 wt% MgO and 1450–1550 °C, respectively (Waterton *et al.*, 2017; Nicklas *et al.*, 2019; Puchtel *et al.*, 2020; Herzberg, 2022). Phanerozoic Gorgona komatiites formed at liquidus temperatures between ~1330–1400 °C from melts with ~17–20 wt% MgO (Révillon *et al.*, 2000; Kamenetsky *et al.*, 2010), though several Phanerozoic picrites record higher liquidus temperatures, ranging up to 1570 °C (Trela *et al.*, 2017).

4.2.2 Komatiite mantle source temperatures

Temperatures of komatiite mantle sources are typically compared using mantle potential temperatures, T_p, the extrapolation of the temperature at the source region to the surface along the solid mantle adiabat (McKenzie and Bickle, 1988). This allows comparison of the thermal anomaly required to produce komatiites sourced from different depths. These are closely related to the pressure of melting because higher

temperature mantle begins to melt at higher pressures during decompression.

One method for calculating T_p involves projecting the komatiite liquidus temperature to the melting region along the adiabatic gradient of komatiitic magma, correcting for the latent heat of melting (McKenzie and Bickle, 1988; Nisbet *et al.*, 1993). The komatiite source T_p is then calculated as the T_p of the mantle adiabat required to intersect the solidus at that depth. This method is highly model dependent, relying on a number assumptions about the style of melting, where the melt separated from its solid mantle source, and whether the magmas lost heat to their wall rocks, or underwent viscous heating as gravitational potential energy is released during their ascent (Nisbet *et al.*, 1993; Sossi *et al.*, 2016). Large uncertainties are also introduced due to the similarity of adiabatic gradients to the solidus gradient at high pressure (Herzberg and O'Hara, 2002) and uncertainties surrounding the exact nature of the high pressure solidus (Andrault *et al.*, 2018).

Alternatively, potential temperatures can be estimated from komatiite melt compositions. This approach uses relationships between the pressure of melting and melt composition, with higher pressures of melting requiring higher T_p to intersect the solidus at greater depths. For example, melt MgO contents largely depend on the depth of melting initiation and, in turn, mantle potential temperature (Herzberg and O'Hara, 2002; Herzberg *et al.*, 2007; Herzberg and Asimow, 2008). The T_p calculated from a given pressure of melting depends on the nature of the solidus. Recent 'low temperature' solidus parameterisations (Andrault *et al.*, 2018) imply relatively low T_p of ~1530 °C for Archaean komatiites, with melting beginning at up to 25 GPa (Pierru *et al.*, 2022). It is presently unclear how such low T_p mantle can produce melts that arrive near the surface with the high liquidus temperatures observed for komatiites, and this merits further investigation. By contrast, more conventional 'high temperature' solidus parameterisations imply higher absolute T_p of ~1700–1900 °C for Archaean komatiites (Herzberg, 2022), though melting begins at lower pressures (~10 GPa; Herzberg and Asimow, 2015).

4.2.3 Are plumes required to form komatiites?

Komatiite liquidus temperatures are mostly significantly higher than those from ambient mantle melts (e.g., Green *et al.*, 1975; Herzberg, 2022). These provide minimum estimates for the komatiite source T_p, because melting always results in a fall in temperature. Notwithstanding the issues outlined above, mantle potential temperature estimates tell a similar story. Almost all komatiites require sources that are far hotter than ambient mantle, with T_p estimates ranging up to 1900 °C (Nisbet *et al.*, 1993; Herzberg *et al.*, 2010). This means that komatiite formation requires the presence of thermally anomalous mantle, ruling out models in which komatiites form at ambient temperatures in mantle refertilised by delamination (Bédard, 2006) or in slab windows (Serrano *et al.*, 2011). We conclude that thermally anomalous mantle plumes are required to form komatiites.

4.3 Are komatiite sources enriched or depleted?

Variations in incompatible trace element ratios and patterns indicate that some komatiites formed from sources that had been depleted by prior melt extraction and others from sources that had undergone some form of enrichment (metasomatism or incorporation of recycled material). Al-enriched, low TiO_2 komatiites are generally derived from the most depleted sources, as recorded in their extremely low concentrations of the more incompatible elements. The mantle-normalized trace element patterns of komatiites from the Commondale region, for example, show a continuous slope from a maximum at Lu to extremely low values for Th (**Figure 5**; Wilson, 2019). Their elevated Al_2O_3/TiO_2 ratios largely reflect depletions in Ti (Kamber and

Tomlinson, 2019). Further evidence of depletion is provided by anomalously elevated concentrations of Ru relative to Pt and Pd, which require that the source had undergone significant (>10%) prior melt extraction (Waterton *et al.*, 2021).

Most Al-depleted and Al-undepleted komatiites vary between primitive mantle-like $(La/Sm)_N$ and moderately depleted $(La/Sm)_N$, consistent with fertile to moderately depleted mantle sources (**Figure 4d**). Interestingly, source depletion appears to be more dependent on the komatiite age rather than type (**Figure 5**). Komatiites older than 3 Ga generally have flat trace element patterns, regardless of whether they are Al-depleted or Al-undepleted, whereas komatiites formed at ~2.7 Ga (predominantly Al-undepleted) have depleted trace element patterns. Al-undepleted and Al-depleted komatiites with more enriched trace-element compositions do exist, though in many cases this results from crustal contamination (Barnes *et al.*, 2021).

Ti-enriched komatiites show wide variations in source enrichment or depletion. Some, such as the Boston Creek komatiite, are LREE-enriched with high concentrations of Fe and Ti. This likely reflects relatively low degree partial melting of a source enriched in both Fe and incompatible trace elements (Stone *et al.*, 1995). Others, such as Proterozoic komatiites from the Baltic Shield, show characteristic 'hump-shaped' REE patterns in which both LREE and HREE are depleted relative to the MREE, consistent with melting of a depleted source with residual garnet (Barnes and Often, 1990; Hanski *et al.*, 2001).

4.4 Degree of melting

The high temperatures inferred for komatiites have led to the suggestion that their mantle sources underwent large degrees of partial melting (Nesbitt *et al.*, 1979; Nisbet, 1982; Herzberg, 1992; Nisbet *et al.*, 1993). Concentrations of moderately incompatible elements, such as Ti, provide information on the percentage of partial melting, as these elements are little affected by source depletion or garnet fractionation. At high degrees of melting, Ti concentrations are inversely proportional to the degree of melting. Using measured TiO_2 contents (**Figure 4a**) and assuming a primitive mantle source with 0.18 wt% TiO_2 (Hofmann, 1988), we estimate that the degree of partial melting for Al-depleted komatiites was between 30–45%, similar to previous estimates (e.g., Herzberg, 1992; Sossi *et al.*, 2016). If Al-undepleted komatiites formed by melting of a primitive mantle-like source, the estimated degree of melting ranges from ~30% to an unrealistic 80%. Use of a depleted mantle source with 0.13 wt% TiO_2 (Salters and Stracke, 2004) reduces the maximum degree of partial melting for these komatiites to a still-high 43% (Waterton *et al.*, 2021). The enigmatic Barberton Al-undepleted komatiites show an unusual combination of extremely low trace element concentrations (~0.22 wt% TiO_2) with no evidence of source depletion, implying an implausible 80% partial melting of a primitive mantle source.

4.5 Depths and pressures of melting

Several lines of reasoning suggest that komatiites form at great depths in the mantle. The MgO contents of near-solidus melts increase with the depth of melting, and do not significantly change with continued adiabatic decompression melting (Herzberg and O'Hara, 2002). Melts with up to 30 wt% MgO require that melting started around 10 GPa unless their sources are considerably depleted. Similarly, projections of the liquidus temperatures of komatiites intersect the mantle solidus only at very high pressures in the upper mantle, if at all (Miller *et al.*, 1991a; Nisbet *et al.*, 1993). The high degrees of melting inferred for komatiites also imply deep melting initiation, because the amount of decompression melting is limited by the decrease in pressure after the source crosses the solidus. Finally, the presence of garnet signatures in Al-depleted

komatiites (Al- and HREE-depletion) places additional constraints on their pressure of melting, discussed below.

4.5.1 Physical constraints on melting depth

For adiabatic decompression melting to occur, the solidus must be steeper (in temperature/pressure) than the adiabatic temperature gradient. In the lower part of the upper mantle the solid adiabat may be slightly steeper or parallel to the fertile peridotite solidus (Miller *et al.*, 1991a), leading McKenzie (2020) to argue that no decompression melting could occur in this region. This depends on the exact solidus used; recent analyses find it to be slightly steeper than the solid adiabat at all upper mantle depths, except for across major phase transitions (Andrault *et al.*, 2018). Regardless, the adiabat and solidus are nearly parallel between ~13–24 GPa, or depths of ~400–670 km, and at most only small degrees of melt can be produced in this region (Nisbet, 1982; Sossi *et al.*, 2016). For large quantities of melt to be present at these depths, it must have formed through melting deeper in the mantle. Furthermore, the major phase transitions bridgmanite to ringwoodite+majorite, ringwoodite to wadsleyite, and wadsleyite to olivine are all endothermic for rising mantle at the temperatures relevant to komatiite formation (Herzberg and Zhang, 1996; Hirose, 2002). These endothermic transitions may further restrict decompression melting in the transition zone, as rising mantle will cool more than predicted from adiabatic gradients alone. This does not preclude small degrees of hydrous melting in or above the mantle transition zone (Myhill *et al.*, 2017; Drewitt *et al.*, 2022), if water is released during these phase transitions (Sobolev *et al.*, 2016; Wilson and Bolhar, 2022). However, high degrees of melting through adiabatic decompression can only be achieved at pressures <13 GPa, or within the lower mantle, where the solidus is significantly steeper than mantle adiabats (McKenzie, 2020).

4.5.2 Did komatiites form in the lower mantle?

McKenzie (2020) proposed that the low trace element contents and high MgO contents of komatiites could be a result of small degrees of melting with residual Ca-perovskite in the uppermost lower mantle. Although his model reproduces average komatiite REE compositions, the fit is poor for most other elements, notably the HFSE. Melts formed in equilibrium with Ca-perovskite should show large positive anomalies of Nb and Ta relative to the REE, because these elements are incompatible in both Ca-perovskite and bridgmanite. This is not observed in most komatiites; the mismatch in the McKenzie (2020) models is masked by the inclusion of some Nb and Ta rich Al-depleted Barberton komatiites in the average komatiite composition modelled (Sossi *et al.*, 2016), that appear highly unusual (c.f., Robin-Popieul *et al.*, 2012; Puchtel *et al.*, 2013). Similarly, the compatibility of Hf and Zr in bridgmanite relative to the REE produces strong negative Zr and Hf anomalies in the McKenzie (2020) models. These features are also not observed in most komatiites. In a related model, Pierru *et al.* (2022) invoked preferential melting of Ca-perovskite in the lower mantle with residual bridgmanite to explain the high CaO/Al_2O_3 of Al-depleted komatiites, though at higher degrees of melting. Again, this does not appear to be compatible with the lack of HFSE/REE fractionation observed in most komatiites, and we note that CaO/Al_2O_3 comparable to typical Al-depleted komatiites (Robin-Popieul *et al.*, 2012) have been experimentally produced at much lower pressures (Walter, 1998).

Another line of evidence against komatiite formation in the lower mantle comes from the highly siderophile elements (HSE; Re, Au, and the platinum-group elements). With increasing pressure, major mantle minerals preferentially incorporate Fe^{3+} over Fe^{2+}, leading to stabilisation of metallic alloys at pressures > 8 GPa (O'Neill *et al.*, 1993; Frost *et al.*, 2004; Rohrbach *et al.*, 2007, 2011). Small degree melts formed in the lower mantle should therefore be virtually devoid of HSE, due to their extremely high partition coefficients in metallic phases. By contrast, komatiites have the highest HSE contents of mantle derived melts (Barnes *et al.*, 2015),

requiring high degrees of melting (Barnes *et al.*, 1985; Waterton *et al.*, 2021). We conclude that melts from the lower mantle did not significantly contribute to komatiite formation, or that the geochemical signatures of these melts were effaced during subsequent ascent of the magmas. Given the arguments that Ca-perovskite was not an important residual phase, high degrees of melting are indeed necessary to explain the low trace element contents of komatiites.

4.5.3 Melting pressures of different komatiite types

Major constraints on komatiite source pressures come from their MgO contents, their high degrees of partial melting, and the presence or absence of garnet signatures (Al- and HREE-depletion), which vary between different komatiite groups. In Al-depleted komatiites, the garnet signature provides a constraint on the pressure of melting (Green, 1975; Ohtani, 1990; Herzberg, 1992) but its application depends on phase relations, particularly the positions of the solidus and the garnet-out curve (**Figure 7a**). Garnet is only retained in residues of 30–45% melting for final pressures of melting >4.5 GPa (Walter, 1998) or >7 GPa (Herzberg and Zhang, 1996; Herzberg *et al.*, 2000). However, higher pressures than these are required to retain enough garnet in the source to match the low Al_2O_3/TiO_2 (~10) of Al-depleted komatiites. Experimental batch melts at melt fractions >30% have $Al_2O_3/TiO_2 \approx 10$ at pressures ≥7 GPa (Walter, 1998), suggesting the majority of melts contributing to the formation of Al-depleted komatiites are sourced from at least this pressure. Alternatively, simple mass balance calculations show that Komati formation Al-depleted komatiites (4.5 wt% Al_2O_3; **Figure 4**) formed from primitive mantle (4.1 wt% Al_2O_3; Hofmann, 1988), with garnet (22 wt% Al_2O_3; Walter, 1998) as the sole aluminous phase in the residue, require the residue to comprise ~20% garnet. This condition is met for >30% melting at pressures $\gtrsim$10 GPa using the phase relations shown (**Figure 7a**). These estimates are consistent with typical parental melt MgO contents of ~30 wt% (Robin-Popieul *et al.*, 2012; Puchtel *et al.*, 2013; Sossi *et al.*, 2016), which indicate that the solidus was crossed at pressures $\gtrsim$10 GPa (Herzberg and Asimow, 2015).

Al-undepleted komatiites lack garnet signatures. This could either reflect a large portion of the melt formed at low pressures, or melting continued beyond garnet exhaustion at higher pressures (**Figure 7b**; Heinonen *et al.*, 2022). Typical Archaean Al-undepleted komatiites have parental melts with ~27–30 wt% MgO (Arndt *et al.*, 2008; Sossi *et al.*, 2016; Nicklas *et al.*, 2018); for dry, fertile sources, this would also indicate pressures for the start of melting $\gtrsim$8 GPa. The common evidence for minor source depletion and the presence of H_2O in some Al-undepleted komatiites (Shimizu *et al.*, 2001; Sobolev *et al.*, 2016) complicates this. Proterozoic and Phanerozoic Al-undepleted komatiites with lower MgO contents likely originate from lower pressures (<5 GPa; Révillon *et al.*, 2000; Waterton *et al.*, 2021; Herzberg, 2022).

The melting pressure of Al-enriched komatiites is not well constrained due to their highly depleted, refractory source compositions. Refractory mantle begins to melt at a shallower depth at a given potential temperature, and will have a higher MgO content at a given depth of melting initiation (Herzberg and O'Hara, 2002). However, Commondale komatiites contain olivine with exceptionally high Al_2O_3 contents (~0.3 wt%), requiring crystallisation pressures >6 GPa and possibly as high as 10 GPa (Agee and Walker, 1990; Wilson and Bolhar, 2022). If, as suggested by Wilson and Bolhar (2022), these are inverted wadsleyite grains, they may have initially crystallised at pressures >15 GPa.

Ti-enriched komatiites generally show garnet signatures (Barnes and Often, 1990; Stone *et al.*, 1995; Hanski *et al.*, 2001), indicating pressures at least some melt was derived from pressures >3 GPa. However, these generally have lower MgO contents and greater incompatible element enrichment than other komatiite types, likely indicating lower degrees of melting at lower pressures.

The depths at which komatiites segregate from their sources are poorly constrained. Al-depleted and some Ti-enriched komatiites are the exception here; to retain residual garnet signatures, they can only have mixed with a small proportion of low-pressure melts and had limited interaction with low-pressure mantle rocks. In modern plumes, melting ceases at the base of the lithosphere, though final pressures of melting may instead reflect the depths at which melts become channelised and effectively isolated from the surrounding upwelling mantle (Herzberg *et al.*, 2023). For Al-depleted komatiites with final pressures of melting >7 GPa, the melts had to segregate well before reaching the base of the lithosphere, and a mechanism for isolating these melts during their ascent is required. For Al-undepleted or Al-enriched komatiites, which lack garnet signatures, melting will drastically slow as fusible components are exhausted from the mantle source (Bernstein *et al.*, 2007). For these komatiites, crossing the garnet-out curve at >6 GPa (T_p ~1800 °C) leaves a dunite residue (Walter, 1998; Herzberg, 2004). Fractional melting would effectively cease at this point (**Figure 7**), though further melting is possible if some melt is retained in the source. However, a lack of unequivocal signatures of high pressure melt segregation means that Al-undepleted or Al-enriched komatiites may have undergone extensive melt-rock reaction during their ascent (Walsh *et al.*, 2023), and formation of a dunite residue does not necessarily correspond to the segregation and isolation of these melts from the surrounding mantle. At lower pressures, melting past garnet-out leaves harzburgite or lherzolite residues (Walter, 1998; Herzberg, 2004), allowing melting to continue at a reduced rate (Asimow *et al.*, 1997).

4.6 Did komatiites form by batch melting?

Batch melting refers to a process during which melts and residues remain in contact until a large melt fraction accumulates. Modern mantle melts do not form via batch melting because, in the shallow mantle, melts are less dense than their solid residues and the melts are interconnected at all melt fractions, meaning they can migrate freely. Picritic melts can be extracted at melt fractions as low as 1% (McKenzie, 1985), implying they form via critical melting (i.e., near-fractional melting with some melt retained with the mantle residue; Maaløe, 1982). However, it is possible that melt migration could be restricted at higher pressures either by low melt interconnectivity (Sossi *et al.*, 2016), or small density differences between komatiite melts and mantle solids (Stolper *et al.*, 1981), potentially permitting batch-like melting to occur.

High-pressure melting experiments show that melts are interconnected along grain boundaries at low melt fractions at pressures up to those of the mantle transition zone (Yoshino *et al.*, 2007; Freitas *et al.*, 2017; Andrault *et al.*, 2018). Given extremely low melt viscosities of 0.005–0.1 Pa·s at conditions relevant to komatiite formation (Ohtani and Suzuki, 1996; Liebske *et al.*, 2005; Xie *et al.*, 2021), komatiites should be able to move freely throughout the upper mantle, providing they are sufficiently buoyant. However, silicate melts are more compressible than solid silicate minerals, leading to density inversions at depth (Stolper *et al.*, 1981). Most importantly, komatiitic melts are denser than olivine in the window from ~8–15 GPa (**Figure 8**), though it is unclear whether they ever become denser than bulk peridotite (Agee and Walker, 1988, 1993; Miller *et al.*, 1991b; Agee, 1998; Schmeling and Arndt, 2017).

These density inversions are the basis of models suggesting that Al-depleted komatiites form by critical melting with high melt-retention (Robin-Popieul *et al.*, 2012), or that all komatiites form by batch melting (Sossi *et al.*, 2016). The negative buoyancy of komatiite melt relative to olivine between 8–15 GPa can potentially cause melt to accumulate in the plume until it ascends to levels where the melt becomes less dense than all solid mantle phases. At this stage the melt escapes the source, departing in a single pulse to produce Al-depleted komatiites (Robin-Popieul *et al.*, 2012; Schmeling and Arndt, 2017). Alternatively, Sossi *et al.* (2016) proposed that in the region where the melt has near-neutral buoyancy, it would migrate upwards

within the plume at velocities significantly less than the plume ascent rate, allowing batch melting to occur. However, we note that measured melt viscosities (Ohtani and Suzuki, 1996; Liebske *et al.*, 2005; Xie *et al.*, 2021) are ~10 – 200 times lower than those used by Sossi *et al.* (2016). This means that komatiite ascent velocities should be faster than the plume ascent rate, except for a very small window around a putative level of neutral buoyancy at ~15 GPa (**Figure 8**).

Geochemical evidence for batch melting in the formation of komatiites is equivocal. Co-variations between incompatible trace elements and radiogenic isotopes (Sossi *et al.*, 2016) only establish the timing of source depletion, and not the melting process that operated (i.e., batch or critical). The FeO concentrations of Al-undepleted komatiites are better matched by batch melting models than fractional, though the inverse is true for SiO_2 contents (Herzberg, 2016). Finally, for high degree melts, incompatible trace element concentrations for batch and pooled critical melts are similar, providing all melts within the melting column are able to effectively mix into the pooled melt (Plank and Langmuir, 1992). However, it is not easy to envisage how near-fractional melts formed over such large melting columns can mix without any loss of melt, and models invoking pooled critical melts must address this.

5 Komatiite formation models

The discussion above rules out the majority of komatiite formation models shown in **Figure 6**. Komatiites form by high degrees of melting in dry or damp, thermally anomalous mantle plumes (e.g., Green *et al.*, 1975; Nesbitt *et al.*, 1979; Herzberg, 1992; Arndt *et al.*, 2008; Sobolev *et al.*, 2016). The available data are unable to distinguish whether komatiites formed from plumes sourced at the core mantle boundary (e.g., Arndt *et al.*, 2008) or in the transition zone (Wyman, 2020). Melting is likely to occur through critical melting, though some mechanism is needed to aggregate and mix critical melts formed over large depth ranges. The wide variations in komatiite geochemistry reflect formation from mantle sources that had undergone varying degrees of depletion and enrichment, combined with variable depths of melting, even within single plumes (Arndt *et al.*, 1977; Révillon *et al.*, 2000). This variability means that care must be taken when using komatiites to trace secular variations in mantle geochemistry (c.f., Maier *et al.*, 2009; Amsellem *et al.*, 2019; Nicklas *et al.*, 2019).

5.1 Al-depleted komatiites

Models for the formation of Al-depleted komatiites must account for residual garnet signatures at high degrees (30–45%) of partial melting, and high parental melt MgO contents (~30 wt%). Two such models komatiites are shown in **Figure 9**. The pressure of melt segregation was ≥7 GPa, but could have been higher than ~10 GPa depending on the phase relations and solidus used (Herzberg and Zhang, 1996; Walter, 1998; Herzberg *et al.*, 2000). As Al-depleted komatiites frequently show little evidence of prior melt depletion, melting initiation occurred at >10 GPa for melts with ~30 wt% MgO (Herzberg and O'Hara, 2002; Herzberg and Asimow, 2015; Sossi *et al.*, 2016).

In model 1, melting begins at ~11 GPa (the approximate intersection of the 30 wt% MgO isopleth with the solidus; **Figure 7**), and melts become isolated by around ~7 GPa. Melts formed over this depth range aggregate and mix during melting and magma ascent (Gurenko and Chaussidon, 1995), either as shallow forming melts are added to upwards migrating deep-formed melts, or as the melts ascend through magma channels. Deep-sourced modern melts appear to be well-mixed relative to shallow-sourced melts (Rudge *et al.*, 2013; Jennings *et al.*, 2017), and it is likely that the long transport pathways of deep-sourced komatiites promotes mixing of melts formed over these large (~150 km) depth ranges.

In model 2, melting begins in a hotter plume with a T_p around 1900°C at significantly greater depths, potentially in the lower mantle. High degrees of melting are reached below ~15 GPa, where wadsleyite with a density close to 3700 kg m^{-3} replaces olivine with a density of about 3400 kg m^{-3} (**Figure 8**). At this point, the melt has a density higher than olivine but less than that of solid peridotite. Schmeling and Arndt (2017) numerically modelled melt migration under these conditions, finding that the reduction in density contrast at ~15 GPa leads to a drop in the velocity of melt migration and accumulation of melt at this depth. The build-up of melt persists as the plume rises, until increasing buoyancy of the melt allows it to escape. These calculations were made using an unrealistically high melt viscosity of 40 Pa s, but new calculations made using 30 mPa s produce similar results (Harro Schmeling, personal communication).

5.2 Archaean Al-undepleted komatiites

Aside from their chondritic Al_2O_3/TiO_2 and Gd/Yb, key features of Archaean Al-undepleted komatiites are their commonly depleted trace element patterns (particularly in ~2.7 Ga komatiites; **Section 4.3**), and the observation that at least some contain appreciable water contents (**Section 4.1**). Al-undepleted komatiites also show consistently depleted Nd isotopic compositions. However, the range measured Sm/Nd ratios in Al-undepleted komatiites is greater than the time integrated Sm/Nd ratios implied by their isotopic compositions (Puchtel *et al.*, 2022). This suggests that at least some of the variation in their source depletion immediately preceded their formation.

We suggest that these features can be explained if plumes rising through or from the mantle transition zone undergo a small amount of hydrous melting when wadsleyite converts to olivine at ~15 GPa (Sobolev *et al.*, 2016; Wilson and Bolhar, 2022). Below this pressure, all mantle adiabats relevant to komatiite formation lie at higher temperatures than the wet solidus (**Figure 7b**). Any water released as wadsleyite, which has a high water storage capacity, coverts to nominally anhydrous olivine, will drive small degrees of flux melting. This early hydrous melting stage begins to deplete the rising mantle in incompatible trace elements and water, though not all water is exhausted from the residue. After this initial stage of melting, there is a hiatus before the onset of adiabatic decompression melting at shallower depths (<10 GPa, or 300 km), producing komatiitic melt. Final pressures of melt segregation are unclear, but must lie either on, or to the low-pressure side of, the garnet-out curve. This observation helps explain why Al-undepleted komatiites generally have lower absolute trace element concentrations and higher calculated degrees of melting than Al-depleted komatiites – for a given MgO content (pressure of melting initiation), higher degrees of melting are required to exhaust garnet in the residue.

The ~3.5 Ga Komati formation Al-undepleted komatiites have flat trace element patterns coupled with extremely low concentrations of these elements (**Figure 5**). They do not appear to have undergone an early stage of hydrous melt depletion. We speculate that this could reflect a drier transition zone at ~3.5 Ga, such that melting only began at the dry solidus. However, we are presently unable to explain formation of these komatiites, which could record the operation of a melting process unique to the Palaeoarchaean.

5.3 Al-enriched, Ti-depleted komatiites

The highly depleted sources of Al-enriched komatiites make it difficult to establish their exact melting depths, and in turn their mode of formation. Tomlinson and Holland (2021) demonstrated that these komatiites could form through melting of depleted, Si- and Al-enriched peridotite, similar to that found in the Kaapvaal mantle

lithosphere. This source may have been produced by melt-rock reactions with earlier komatiitic melts (Tomlinson and Kamber, 2021), or by extensive prior melt depletion (Wilson *et al.*, 2003; Wilson, 2019; Waterton *et al.*, 2021). The identification of olivine crystallised at pressures of ~10 GPa in the Al-enriched Commondale komatiites, indicates at least some Al-enriched komatiites formed through deep melting in mantle plume (Wilson and Bolhar, 2022), and that ultra-depleted mantle domains existed in the Archaean convecting mantle (Stracke *et al.*, 2019).

5.4 Ti-enriched and post-Archaean komatiites

Al-undepleted komatiites younger than ~2 Ga formed by lower degrees of melting, at pressures and mantle temperatures comparable to some modern picrites (Trela *et al.*, 2017; Waterton *et al.*, 2021). Phanerozoic komatiites from Gorgona Island formed in a zoned plume in which various picrites and komatiites formed from variably depleted sources. The picrites may have formed through melting a depleted source residual to komatiite formation (Kerr *et al.*, 1996; Révillon *et al.*, 2000). Similar processes may have operated in the Archaean, explaining why some greenstone belts contain several types of komatiite formed in the same magmatic events (Sproule *et al.*, 2002; Robin-Popieul *et al.*, 2012).

Ti-enriched komatiites also formed at relatively low pressures and temperatures, with correspondingly lower degrees of melting than other komatiites. Those formed by low-degree partial melting of enriched sources may be more akin to ferropicrites than komatiites (Stone *et al.*, 1995), with mantle metasomatism potentially explaining the high water contents inferred from igneous amphibole in some Ti-enriched komatiites (Stone *et al.*, 1997).

6 Future directions

Despite the progress made in the past 20 years, a number of fundamental questions remain regarding the formation of komatiites. Many of these relate to the physical and chemical characteristics of deep melting, where even basic properties such as the location of the mantle solidus are debated (Walter, 1998; Herzberg *et al.*, 2000; Andrault *et al.*, 2018). How melts segregate and migrate to the surface is still under question (Sossi *et al.*, 2016; Schmeling and Arndt, 2017; McKenzie, 2020), and the effects of melt-rock reactions on komatiites and the mantle they ascend through is only just beginning to be addressed (Tomlinson and Kamber, 2021; Walsh *et al.*, 2023). The implications of a komatiite-forming mantle also remain up for debate; how do mantle dynamics and tectonics operate in mantle where the hottest parts are capable of producing melts with liquidus temperatures up to ~1600 °C (Fischer and Gerya, 2016)? Finally, questions remain around the occurrence of komatiites and their link to the thermal evolution of the mantle. While a first-order decrease in the abundance of komatiites throughout Earth history is consistent with secular mantle cooling, the apparent absence of komatiites in the Eoarchaean and much of the Proterozoic, and modern melts with temperatures approaching those of komatiites (Trela *et al.*, 2017), complicate this simple view. Progress on these questions will ensure the next 20 years of komatiite research remains just as vibrant as the past 20.

Acknowledgements

This manuscript greatly benefitted from discussions with Igor Puchtel, Claude Herzberg, Allan Wilson, Stephane Labrosse, Denis Andrault, Edward Stolper, Paolo Sossi, Cinzia Farnetani, Eiji Ohtani, Tatsuya Sakamaki. We additionally thank Claude Herzberg for allowing us to modify his mantle phase diagrams for **Figure 7** of this chapter, and Claude Herzberg and Rémy Pierru for constructive reviews. PW was supported

by VILLUM FONDEN through Grant VKR18978.

Figures

Figure 1: Morphology of komatiite flows and deposits, modified from Pyke *et al.* (1973), Arndt and Fleet (1979), and Arndt *et al.* (2008).

Figure 2: **a)** Transition between random olivine spinifex (top) and platy olivine spinifex (bottom) in a differentiated komatiite flow, Komati Formation, Barberton Greenstone Belt. **b)** Dendritic pyroxene and devitrified glass (sometimes misidentified as 'microspinifex') interstitial to olivine phenocrysts, from a massive flow, Winnipegosis komatiites, Canada. **c)** 'Jackstraw textured' metamorphic olivine (dark bladed mineral) from amphibolite facies olivine-talc-serpentine metamorphic rocks, Saglek Gneiss, northern Labrador.

Figure 3: Histograms showing the relative abundance of komatiite through Earth history. **a)** Raw frequency of komatiite analyses from the GEOROC database (n ≈ 3660, DIGIS Team, 2022). **b)** Same analyses normalised to a global database of detrital zircon analyses, to correct for periods of increased crustal production and/or preservation, for example at 2.7 Ga. Zircon data for normalisation are 'best ages' from Puetz and Condie (2019), filtered for <10% discordance (n ≈ 515,000). Some komatiite localities are overrepresented (e.g., the 3.5 Ga peak largely reflects intensive study of the Barberton komatiites), while other localities may only have approximate ages, or are questionably identified as komatiites. As such, these abundances are only intended to be illustrative. However, the zircon normalised plot shows that the abundance of 2.7 Ga komatiites is, in part, due to increased crustal production or preservation at that time.

Figure 4: **a)** Komatiite discrimination plot of $(TiO_2)_{25}$ against $(Al_2O_3)_{25}$. **b)** Calculation of $(Al_2O_3)_{25}$ by interpolating or extrapolating regressions of Al_2O_3 against MgO to 25 wt% MgO. **c)** Al_2O_3/TiO_2 vs $(Gd/Yb)_N$ diagram after Jahn *et al.* (1982). **d)** $(Gd/Yb)_N$ vs $(La/Sm)_N$ diagram, along with simplified REE patterns for some of the komatiites. Data sources: Komati ADK and Weltevreden (Puchtel *et al.*, 2013); Ruth Well-Regal, Komati AUK, Belingwe, Munro, Yilgarn (Sossi *et al.*, 2016), Winnipegosis (Waterton *et al.*, 2017), Kambalda (Lesher and Arndt, 1995), Kostomuksha (Puchtel *et al.*, 1998), Gorgona komatiites and picrites (Révillon *et al.*, 2000), Commondale (Wilson, 2019), Jeesiörova (Hanski *et al.*, 2001), Boston Creek (Puchtel *et al.*, 2018).

Figure 5: Komatiite trace element patterns, normalised to primitive mantle (Hofmann, 1988) and grouped by age or type. Note different scale for Al- and Ti-enriched komatiites. Komati formation, Regal-Ruth Well, Coonterunah, Belingwe and Yilgarn patterns are parental melt compositions estimated by Sossi *et al.* (2016). Patterns for Alexo (Lahaye and Arndt, 1996), Commondale (Wilson, 2019), Weltevreden (Puchtel *et al.*, 2013), Boston Creek (Puchtel *et al.*, 2018), Jeesiörova (Hanski *et al.*, 2001), Winnipegosis (Waterton *et al.*, 2017) and Gorgona (Révillon *et al.*, 2000), are representative samples that approximate liquid compositions. ADK = Al-depleted, AUK = Al-undepleted, AEK = Al-enriched, Ti = Ti-enriched.

Figure 6: Komatiite formation model 'tree' showing a hierarchy of major models proposed for komatiites, along with references for prominent advocates of each model (Green, 1972; Parman *et al.*, 1997; Révillon *et al.*, 2000; Shimizu *et al.*, 2001; Bédard, 2006; Serrano *et al.*, 2011; Herzberg, 2016; Sossi *et al.*, 2016; McKenzie, 2020; Wyman, 2020).

Figure 7: Phase diagram of fertile peridotite KLB-1 showing schematic komatiite ascent and melting paths,

modified from a diagram supplied by Claude Herzberg (personal communication). Phase relations and nominally anhydrous solidus are from Herzberg and Zhang (1996) and Herzberg *et al.* (2000). Present day ambient mantle uses adiabatic gradients from Katsura *et al.* (2010) and McKenzie (2020). Schematic komatiite ascent paths and solid adiabat projections for potential temperature (T_p) are assumed to follow paths parallel to ambient mantle before crossing the solidus (dashed lines). Melting (solid lines) and liquid ascent paths (dotted lines) are assumed to be parallel to curves of constant MgO (MgO isopleths, grey lines; Herzberg and O' Hara, 2002; Herzberg and Asimow, 2015). **a)** Pressure of melt segregation for Al-depleted komatiites at two different T_p (coloured stars). To retain a garnet signature at >30% melting (black dashed curve), these must lie to the high-pressure side of the garnet-out curve. Locations of the solidus, liquidus, 30% melting, and garnet-out curve depend on the phase relations used (e.g., Herzberg and Zhang, 1996; Walter, 1998; Herzberg *et al.*, 2000; Andrault *et al.*, 2018); these pressures are necessarily approximate. Projections of the solid adiabat for T_p > 1870 °C intersect the olivine-wadsleyite transition before the solidus; mantle of this temperature would likely begin to melt at the top of the lower mantle (Miller *et al.*, 1991a) and the pressure-temperature path it follows is unclear. **b)** Comparison of komatiite ascent paths with hydrous solidus for 0.1 wt% H_2O (Litasov *et al.*, 2014). At all T_p relevant for the formation of Al-undepleted komatiites, the ascent path is higher than the hydrous solidus. Any water released on breakdown of wadsleyite to olivine will therefore cause minor hydrous melting, before a hiatus once water is exhausted. Melting will then continue at lower pressures at the nominally anhydrous solidus, and final pressures of melt segregation, though poorly constrained, must be either on, or to the low-pressure side of, the garnet-out curve.

Figure 8: Relationship between the densities of solid mantle minerals (~Fo94, Py90 at 2000°C) and molten komatiite (Agee and Walker, 1988; Ohtani *et al.*, 1995; Agee, 1998). The brown dashed line shows the estimated density of mantle peridotite undergoing high degree melting, which is essentially pure olivine at low pressure and 50% garnet, 50% olivine or wadsleyite at 15 GPa. Garnet mode and pressures of phase transitions at temperatures relevant to komatiite formation are from Ishii *et al.* (2018); ringwoodite is less abundant or absent at these temperatures. In the window from about 8 to 15 GPa, komatiite melt is denser than olivine but remains less dense than mantle peridotite.

Figure 9: Models for the formation of Al-depleted komatiites in a plume. In model 1, melting is relatively shallow (~11 – 7 GPa), and melts formed over this depth range accumulate and mix in channels during ascent. Melts become effectively isolated from addition of shallower melts once melt channels become large enough (Herzberg *et al.*, 2023). In model 2, melting is relatively deep (>15 GPa). Melts formed over a wide depth range accumulate and mix at ~15 GPa, where a 'traffic jam' is formed due to slowing melt ascent velocities as wadsleyite converts to olivine. The melts escape in large pulses as they become increasingly buoyant with further decompression (Schmeling and Arndt, 2017).

References

Agee, C. B. (1998). Crystal-liquid density inversions in terrestrial and lunar magmas. *Physics of the Earth and Planetary Interiors* **107**, 63–74.

Agee, C. B. & Walker, D. (1988). Static compression and olivine flotation in ultrabasic silicate liquid. *Journal of Geophysical Research* **93**, 3437–3449.

Agee, C. B. & Walker, D. (1990). Aluminum partitioning between olivine and ultrabasic silicate liquid to 6 GPa. *Contributions to Mineralogy and Petrology* **105**, 243–254.

Agee, C. B. & Walker, D. (1993). Olivine flotation in mantle melt. *Earth and Planetary Science Letters* **114**, 315–324.

Aitken, B. G. & Echeverría, L. M. (1984). Petrology and Geochemistry of Komatiites and Tholeiites from Gorgona-Island, Colombia. *Contributions to Mineralogy and Petrology* **86**, 94–105.

Amsellem, E., Moynier, F. & Puchtel, I. S. (2019). Evolution of the Ca isotopic composition of the mantle. *Geochimica et Cosmochimica Acta* **258**, 195–206.

Andrault, D. *et al.* (2018). Deep and persistent melt layer in the Archaean mantle. *Nature Geoscience*. Springer US **11**, 139–143.

Anh, T. V., Pang, K. N., Chung, S. L., Lin, H. M., Hoa, T. T., Anh, T. T. & Yang, H. J. (2011). The Song Da magmatic suite revisited: A petrologic, geochemical and Sr-Nd isotopic study on picrites, flood basalts and silicic volcanic rocks. *Journal of Asian Earth Sciences*. Elsevier Ltd **42**, 1341–1355.

Arndt, N. & Brooks, C. (1980). Komatiites. *Geology* **8**, 155–156.

Arndt, N., Lehnert, K. & Vasil'ev, Y. (1995). Meimechites: highly magnesian lithosphere-contaminated alkaline magmas from deep subcontinental mantle. *Lithos* **34**, 41–59.

Arndt, N., Lesher, C. M. & Barnes, S. J. (2008). *Komatiite*. Cambridge: Cambridge University Press.

Arndt, N. T. (1977). Ultrabasic magmas and high-degree melting of the mantle. *Contributions to Mineralogy and Petrology* **64**, 205–221.

Arndt, N. T. (1982). Proterozoic spinifex-textured basalts of Gilmour Island, Hudson Bay. *Current Research, Part A, Geological Survey of Canada, Paper 82-1A*. Geological Survey of Canada, 137–142.

Arndt, N. T. (1986). Differentiation of komatiite flows. *Journal of Petrology* **27**, 279–301.

Arndt, N. T. (1994). Archean Komatiites. *Developments in Precambrian Geology* **11**, 11–44.

Arndt, N. T. & Fleet, M. E. (1979). Stable and metastable pyroxene crystallization in layered komatiite lava flows. *American Mineralogist* **64**, 856–864.

Arndt, N. T., Ginibre, C., Chauvel, C., Albarede, F., Cheadle, M., Herzberg, C., Jenner, G. & Lahaye, Y. (1998). Were komatiites wet? *Geology* **26**, 739–742.

Arndt, N. T., Naldrett, A. J. & Pyke, D. R. (1977). Komatiitic and iron-rich tholeiitic lavas of munro township, Northeast Ontario. *Journal of Petrology* **18**, 319–369.

Arndt, N. T. & Nesbitt, R. W. (1982). Geochemistry of Munro Township basalts. In: Arndt, N. T. & Nisbet, E. G. (eds) *Komatiites*. London: George Allen & Unwin, 309–330.

Asafov, E. V., Sobolev, A. V., Batanova, V. G. & Portnyagin, M. V. (2020). Chlorine in the earth's mantle as an indicator of the global recycling of oceanic crust. *Russian Geology and Geophysics* **61**, 937–950.

Asafov, E. V., Sobolev, A. V., Gurenko, A. A., Arndt, N. T., Batanova, V. G., Portnyagin, M. V., Garbe-Schönberg, D. & Krasheninnikov, S. P. (2018). Belingwe komatiites (2.7 Ga) originate from a plume with moderate water content, as inferred from inclusions in olivine. *Chemical Geology*. Elsevier **478**, 39–59.

Asimow, P. D., Hirschmann, M. M. & Stolper, E. M. (1997). An analysis of variations in isentropic melt productivity. *Philosophical Transactions of the Royal Society of London. Series A: Mathematical, Physical and Engineering Sciences*. Royal Society **355**, 255–281.

Ayer, J., Amelin, Y., Corfu, F., Kamo, S., Ketchum, J., Kwok, K. & Trowell, N. (2002). Evolution of the southern Abitibi greenstone belt based on U-Pb geochronology: Autochthonous volcanic construction followed by plutonism, regional deformation and sedimentation. *Precambrian Research* **115**, 63–95.

Barnes, S. J. (2006). Komatiites: Petrology, Volcanology, Metamorphism, and Geochemistry. *Nickel Deposits of the Yilgarn Craton: Geology, Geochemistry, and Geophysics Applied to Exploration*. Society of Economic Geologists, 0.

Barnes, S. J. & Arndt, N. T. (2019). *Distribution and Geochemistry of Komatiites and Basalts Through the Archean*. *Earth's Oldest Rocks*. Elsevier B.V.

Barnes, S. J. & Lesher, C. M. (2008). Physical volcanology. *Komatiite*. Cambridge: Cambridge University Press,

243–294.
Barnes, S. J., Mungall, J. E. & Maier, W. D. (2015). Platinum group elements in mantle melts and mantle samples. *Lithos*. Elsevier B.V. **232**, 395–417.
Barnes, S. J., Naldrett, A. J. & Gorton, M. P. (1985). The origin of the fractionation of platinum-group elements in terrestrial magmas. *Chemical Geology* **53**, 303–323.
Barnes, S. J. & Often, M. (1990). Ti-rich komatiites from northern Norway. *Contributions to Mineralogy and Petrology* **105**, 42–54.
Barnes, S. J., Williams, M., Smithies, R. H., Hanski, E. & Lowrey, J. R. (2021). Trace Element Contents of Mantle-Derived Magmas through Time. *Journal of Petrology* **62**, 1–38.
Bédard, J. H. (2006). A catalytic delamination-driven model for coupled genesis of Archaean crust and sub-continental lithospheric mantle. *Geochimica et Cosmochimica Acta* **70**, 1188–1214.
Bernstein, S., Kelemen, P. B. & Hanghøj, K. (2007). Consistent olivine Mg# in cratonic mantle reflects Archean mantle melting to the exhauston of orthopyroxene. *Geology* **35**, 459–462.
Berry, A. J., Danyushevsky, L. V., St C. O'Neill, H., Newville, M. & Sutton, S. R. (2008). Oxidation state of iron in komatiitic melt inclusions indicates hot Archaean mantle. *Nature* **455**, 960–963.
Bickle, M. J. (1982). The magnesium content of komatiitic liquids. In: Arndt, N. T. & Nisbet, E. G. (eds) *Komatiites*. London: George Allen & Unwin, 479–494.
Brooks, C. & Hart, S. R. (1974). On the Significance of Komatiite. *Geology* **2**, 107–110.
Cameron, W. E. & Nisbet, E. G. (1982). Phanerozoic analogues of komatiitic basalts. In: Arndt, N. T. & Nisbet, E. G. (eds) *Komatiites*. London: George Allen & Unwin, 29–50.
Cameron, W. E., Nisbet, E. G. & Dietrich, V. J. (1979). Boninites, komatiites and ophiolitic basalts. *Nature* **280**, 550–553.
Campbell, I. H. & Arndt, N. T. (1982). Pyroxene accumulation in spinifex-textured rocks. *Geological Magazine*. Cambridge University Press **119**, 605–610.
Campbell, I. H. & Griffin, W. L. (1992). The Changing Nature of Mantle Hotspots through Time: Implications for the Chemical Evolution of the Mantle. *The Journal of Geology* **92**, 497–523.
Campbell, I. H., Griffiths, R. W. & Hill, R. I. (1989). Melting in an Archaean mantle plume: heads it's basalts, tails it's komatiites. *Nature* **342**, 189–92.
Chadwick, B. & Crewe, M. A. (1986). Chromite in the early Archean Akilia association (ca. 3,800 m.y.), Ivisartoq region, inner Godthabsfjord, southern west Greenland. *Economic Geology* **81**, 184–191.
Collerson, K. D., Jesseau, C. W. & Bridgwater, D. (1976). Contrasting types of bladed olivine in ultramafic rocks from the Archean of Labrador. *Canadian Journal of Earth Sciences* **13**, 442–450.
Condie, K. C. & O'Neill, C. (2010). The Archean-Proterozoic boundary: 500 MY of tectonic transition in Earth history. *American Journal of Science* **310**, 775–790.
Coogan, L. A., Saunders, A. D. & Wilson, R. N. (2014). Aluminum-in-olivine thermometry of primitive basalts: Evidence of an anomalously hot mantle source for large igneous provinces. *Chemical Geology* **368**, 1–10.
Dann, J. C. (2000). The 3.5 Ga Komati Formation, Barberton Greenstone Belt, South Africa, Part I: New maps and magmatic architecture. *South African Journal of Geology* **103**, 47–68.
de Wit, M. J., Hart, R. A. & Hart, R. J. (1987). The Jamestown Ophiolite Complex, Barberton mountain belt: a section through 3.5 Ga oceanic crust. *Journal of African Earth Sciences* **6**, 681–730.
DIGIS Team (2022). *2022-12-2JETOA_KOMATIITE.csv, GEOROC Compilation: Rock Types, GRO.data, V5*. .
Donaldson, C. H. (1982). Spinifex textured komatiites: a review of textures, compositions and layering. In: Arndt, N. T. & Nisbet, E. G. (eds) *Komatiites*. London: Allen & Unwin, 213–244.
Drewitt, J. W. E., Walter, M. J., Brodholt, J. P., Muir, J. M. R. & Lord, O. T. (2022). Hydrous silicate melts and the deep mantle H2O cycle. *Earth and Planetary Science Letters*. Elsevier B.V. **581**.
Echeverria, L. M. (1980). Tertiary or Mesozoic komatiites from Gorgona Island, Colombia: Field relations and geochemistry. *Contributions to Mineralogy and Petrology* **73**, 253–266.
Echeverría, L. M. & Aitken, B. G. (1986). Pyroclastic rocks: another manifestation of ultramafic volcanism on Gorgona Island, Colombia. *Contributions to Mineralogy and Petrology* **92**, 428–436.
Evans, B. W. & Trommsdorff, V. (1974). On Elongate Olivine of Metamorphic Origin. *Geology* **2**, 131–132.
Faure, F., Arndt, N. I. & Libourel, G. (2006). Formation of spinifex texture in komatiites: An experimental study. *Journal of Petrology* **47**, 1591–1610.
Fischer, R. & Gerya, T. (2016). Early Earth plume-lid tectonics: A high-resolution 3D numerical modelling

approach. *Journal of Geodynamics*. Elsevier Ltd **100**, 198–214.
Francis, D. (1985). The Baffin Bay lavas and the value of picrites as analogues of primary magmas. *Contributions to Mineralogy and Petrology* **89**, 144–154.
Frank, E. A., Maier, W. D. & Mojzsis, S. J. (2016). Highly siderophile element abundances in Eoarchean komatiite and basalt protoliths. *Contributions to Mineralogy and Petrology*. Springer Berlin Heidelberg **171**, 1–16.
Freitas, D., Manthilake, G., Schiavi, F., Chantel, J., Bolfan-Casanova, N., Bouhifd, M. A. & Andrault, D. (2017). Experimental evidence supporting a global melt layer at the base of the Earth's upper mantle. *Nature Communications*. Springer US **8**, 1–7.
Frost, D. J., Liebske, C., Langenhorst, F., McCammon, C. A., Trønnes, R. G. & Rubie, D. C. (2004). Experimental evidence for the existence of iron-rich metal in the Earth's lower mantle. *Nature* **428**, 409–412.
Gélinas, L., Lajoie, J. & Brooks, C. (1977). Origin and significance of Archean ultramafic volcaniclastics from Spinifex Ridge, La Motte Township, Québec. In: Baragar, W. R. A., Coleman, L. C. & Hall, J. M. (eds) *Volcanic regimes in Canada. Geological Association of Canada, Special Paper No. 16*, 297–309.
Green, D. H. (1972). Archaean greenstone belts may include terrestrial equivalents of lunar maria? *Earth and Planetary Science Letters* **15**, 263–270.
Green, D. H. (1975). Genesis of Archean peridotitic magmas and constraints on Archean geothermal gradients and tectonics. *Geology* **3**, 15–18.
Green, D. H., Nicholls, I. A., Viljoen, M. J. & Viljoen, R. P. (1975). Experimental Demonstration of the Existence of Peridotitic Liquids in Earliest Archean Magmatism. *Geology* **3**, 11–14.
Grove, T. L. & Parman, S. W. (2004). Thermal evolution of the Earth as recorded by komatiites. *Earth and Planetary Science Letters* **219**, 173–187.
Gurenko, A. A. & Chaussidon, M. (1995). Enriched and depleted primitive melts included in olivine from Icelandic tholeiites: origin by continuous melting of a single mantle column. *Geochimica et Cosmochimica Acta* **59**, 2905–2917.
Gurenko, A. A., Kamenetsky, V. S. & Kerr, A. C. (2016). Oxygen isotopes and volatile contents of the Gorgona komatiites, Colombia: A confirmation of the deep mantle origin of H2O. *Earth and Planetary Science Letters*. Elsevier B.V. **454**, 154–165.
Hanski, E., Huhma, H., Rastas, P. & Kamenetsky, V. S. (2001). The Palaeoproterozoic Komatiite – Picrite Association of Finnish Lapland. *Journal of Petrology* **42**, 855–876.
Hanski, E. J. & Smolkin, V. F. (1995). Iron- and LREE-enriched mantle source for early Proterozoic intraplate magmatism as exemplified by the Pechenga ferropicrites, Kola Peninsula, Russia. *Lithos* **34**, 107–125.
Hanski, E., Walker, R. J., Huhma, H., Polyakov, G. V., Balykin, P. A., Hoa, T. T. & Phuong, N. T. (2004). Origin of the Permian-Triassic komatiites, northwestern Vietnam. *Contributions to Mineralogy and Petrology* **147**, 453–469.
Haugaard, R., Waterton, P., Ootes, L., Pearson, D. G., Luo, Y. & Konhauser, K. (2021). Detrital chromites reveal Slave craton's missing komatiite. *Geology* **49**, 1079–1083.
Hauri, E. H., Maclennan, J., McKenzie, D., Gronvold, K., Oskarsson, N. & Shimizu, N. (2018). CO2 content beneath northern Iceland and the variability of mantle carbon. *Geology* **46**, 55–58.
Heinonen, J. S., Brown, E. L., Turunen, S. T. & Luttinen, A. V. (2022). Heavy rare earth elements and the sources of continental flood basalts. *Journal of Petrology*.
Herzberg, C. (1992). Depth and degree of melting of komatiites. *Journal of Geophysical Research* **97**, 4521–4540.
Herzberg, C. (2004). Geodynamic information in peridotite petrology. *Journal of Petrology* **45**, 2507–2530.
Herzberg, C. (2016). Petrological evidence from komatiites for an early Earth carbon and water cycle. *Journal of Petrology* **57**, 2271–2288.
Herzberg, C. (2022). Understanding the Paleoproterozoic Circum-Superior Large Igneous Province constrains the thermal properties of Earth's mantle through time. *Precambrian Research*. Elsevier B.V. **375**, 106671.
Herzberg, C. & Asimow, P. D. (2008). Petrology of some oceanic island basalts: PRIMELT2.XLS software for primary magma calculation. *Geochemistry, Geophysics, Geosystems* **9**.
Herzberg, C., Asimow, P. D., Arndt, N., Niu, Y., Lesher, C. M., Fitton, J. G., Cheadle, M. J. & Saunders, A. D. (2007). Temperatures in ambient mantle and plumes: Constraints from basalts, picrites, and komatiites. *Geochemistry, Geophysics, Geosystems* **8**.
Herzberg, C., Condie, K. & Korenaga, J. (2010). Thermal history of the Earth and its petrological expression.

Earth and Planetary Science Letters. Elsevier B.V. **292**, 79–88.
Herzberg, C. & O'Hara, M. J. (2002). Plume-Associated Ultramafic Magmas of Phanerozoic Age. *Journal of Petrology* **43**, 1857–1883.
Herzberg, C., Raterron, P. & Zhang, J. (2000). New experimental observations on the anhydrous solidus for peridotite KLB-1. *Geochemistry, Geophysics, Geosystems* **1**.
Herzberg, C. T. & Asimow, P. D. (2015). PRIMELT3 MEGA.XLSM software for primarymagma calculation: Peridotite primarymagma MgO contents fromthe liquidus to the solidus. *Geochemistry, Geophysics, Geosystems* **16**, 563–578.
Herzberg, C. T., Asimow, P. D. & Hernández-Montenegro, J. D. (2023). The Meaning of Pressure for Primary Magmas: New Insights From PRIMELT3-P. *Geochemistry, Geophysics, Geosystems* **24**.
Herzberg, C. & Zhang, J. (1996). Melting experiments on anhydrous peridotite KLB-1: Compositions of magmas in the upper mantle and transition zone. *Journal of Geophysical Research: Solid Earth* **101**, 8271–8295.
Hill, R. E. T., Barnes, S. J., Gole, M. J. & Dowling, S. E. (1995). The volcanology of komatiites as deduced from field relationships in the Norseman-Wiluna greenstone belt, Western Australia. *Lithos* **34**, 159–188.
Hirose, K. (2002). Phase transitions in pyrolitic mantle around 670-km depth: Implications for upwelling of plumes from the lower mantle. *Journal of Geophysical Research: Solid Earth* **107**, ECV 3-1-ECV 3-13.
Hofmann, A. W. (1988). Chemical differentiation of the Earth: the relationship between mantle, continental crust, and oceanic crust. *Earth and Planetary Science Letters* **90**, 297–314.
Hole, M. J. & Natland, J. H. (2020). Magmatism in the North Atlantic Igneous Province; mantle temperatures, rifting and geodynamics. *Earth-Science Reviews*. Elsevier **206**.
Hollings, P., Wyman, D. & Kerrich, R. (1999). Komatiite-basalt-rhyolite volcanic associations in Northern Superior Province greenstone belts: Significance of plume-arc interaction in the generation of the proto continental Superior Province. *Lithos* **46**, 137–161.
Ishii, T., Kojitani, H. & Akaogi, M. (2018). Phase relations and mineral chemistry in pyrolitic mantle at 1600–2200 °C under pressures up to the uppermost lower mantle: Phase transitions around the 660-km discontinuity and dynamics of upwelling hot plumes. *Physics of the Earth and Planetary Interiors*. Elsevier **274**, 127–137.
Ivanov, A. V. *et al.* (2018). Volatile concentrations in olivine-hosted melt inclusions from meimechite and melanephelinite lavas of the Siberian Traps Large Igneous Province: Evidence for flux-related high-Ti, high-Mg magmatism. *Chemical Geology*. Elsevier **483**, 442–462.
Jahn, B. ming, Gruau, G. & Glikson, A. Y. (1982). Komatiites of the Onverwacht Group, S. Africa: REE geochemistry, Sm/Nd age and mantle evolution. *Contributions to Mineralogy and Petrology* **80**, 25–40.
Jennings, E. S., Gibson, S. A., Maclennan, J. & Heinonen, J. S. (2017). Deep mixing of mantle melts beneath continental flood basalt provinces: Constraints from olivine-hosted melt inclusions in primitive magmas. *Geochimica et Cosmochimica Acta*. The Author(s) **196**, 36–57.
Kalsbeek, F. & Manatschal, G. (1999). Geochemistry and tectonic significance of peridotitic and metakomatiitic rocks from the Ussuit area, Nagssugtoqidian orogen, West Greenland. *Precambrian Research* **94**, 101–120.
Kamber, B. S. & Tomlinson, E. L. (2019). Petrological, mineralogical and geochemical peculiarities of Archaean cratons. *Chemical Geology*. Elsevier **511**, 123–151.
Kamenetsky, V. S., Gurenko, A. A. & Kerr, A. C. (2010). Composition and temperature of komatiite melts from Gorgona Island, Colombia, constrained from olivine-hosted melt inclusions. *Geology* **38**, 1003–1006.
Katsura, T. *et al.* (2010). Adiabatic temperature profile in the mantle. *Physics of the Earth and Planetary Interiors*. Elsevier B.V. **183**, 212–218.
Kerr, A. C. & Arndt, N. T. (2001). A Note on the IUGS Reclassification of the High-Mg and Picritic Volcanic Rocks. *Journal of Petrology* **42**, 2169–2171.
Kerr, A. C., Marriner, G. F., Arndt, N. T., Tarney, J., Nivia, A., Saunders, A. D. & Duncan, R. A. (1996). The petrogenesis of Gorgona komatiites, picrites and basalts: new field, petrographic and geochemical constraints. *Lithos* **37**, 245–260.
Lahaye, Y. & Arndt, N. T. (1996). Alteration of a Komatiite Flow from Alexo, Ontario, Canada. *Journal of Petrology* **37**, 1261–1284.
Le Bas, M. J. (2000). IUGS reclassification of the high-Mg and picritic volcanic rocks. *Journal of Petrology* **41**, 1467–1470.

Lesher, C. M. & Arndt, N. T. (1995). REE and Nd isotope geochemistry, petrogenesis and volcanic evolution of contaminated komatiites at Kambalda, Western Australia. *Lithos* **34**, 127–157.

Liebske, C., Schmickler, B., Terasaki, H., Poe, B. T., Suzuki, A., Funakoshi, K. ichi, Ando, R. & Rubie, D. C. (2005). Viscosity of peridotite liquid up to 13 GPa: Implications for magma ocean viscosities. *Earth and Planetary Science Letters* **240**, 589–604.

Litasov, K. D., Shatskiy, A. & Ohtani, E. (2014). Melting and subsolidus phase relations in peridotite and eclogite systems with reduced COH fluid at 3-16 GPa. *Earth and Planetary Science Letters*. Elsevier B.V. **391**, 87–99.

Lofgren, G. E. (1983). Effect of heterogeneous nucleation on basaltic textures: a dynamic crystallization study. *Journal of Petrology* **24**, 229–255.

Lowe, D. R., Drabon, N., Byerly, G. R. & Byerly, B. L. (2021). Windblown Hadean zircons derived by erosion of impact-generated 3.3 Ga uplifts, Barberton Greenstone Belt, South Africa. *Precambrian Research*. Elsevier B.V. **356**, 106111.

Lowrey, J. R., Ivanic, T. J., Wyman, D. A. & Roberts, M. P. (2017). Platy pyroxene: New insights into spinifex texture. *Journal of Petrology* **58**, 1671–1700.

Maaløe, S. (1982). Geochemical aspects of permeability controlled partial melting and fractional crystallization. *Geochimica et Cosmochimica Acta* **46**, 43–57.

Maier, W. D., Barnes, S. J., Campbell, I. H., Fiorentini, M. L., Peltonen, P., Barnes, S.-J. & Smithies, R. H. (2009). Progressive mixing of meteoritic veneer into the early Earth's deep mantle. *Nature*. Nature Publishing Group **460**, 620–623.

Mallmann, G. & O'Neill, H. S. C. (2013). Calibration of an empirical thermometer and oxybarometer based on the partitioning of sc, Y and V between olivine and silicate melt. *Journal of Petrology* **54**, 933–949.

Marsh, B. D. (1981). On the crystallinity, probability of occurrence, and rheology of lava and magma. *Contributions to Mineralogy and Petrology* **78**, 85–98.

Matzen, A. K., Baker, M. B., Beckett, J. R. & Stolper, E. M. (2011). Fe-Mg Partitioning between Olivine and High-magnesian Melts and the Nature of Hawaiian Parental Liquids. *Journal of Petrology* **52**, 1243–1263.

McKenzie, D. (1985). The extraction of magma from the crust and mantle. *Earth and Planetary Science Letters* **74**, 81–91.

McKenzie, D. (2020). Speculations on the generation and movement of komatiites. *Journal of Petrology* **61**, egaa061.

McKenzie, D. & Bickle, M. J. (1988). The volume and composition of melt generated by extension of the lithosphere. *Journal of Petrology* **29**, 625–679.

Miller, G. H., Stolper, E. M. & Ahrens, T. J. (1991a). The equation of state of a molten komatiite 2. Application to komatiite petrogenesis and the Hadean mantle. *Journal of Geophysical Research* **96**, 849–864.

Miller, G. H., Stolper, E. M. & Ahrens, T. J. (1991b). The Equation of State of a Molten Komatiite 1. Shock Wave Compression to 36 GPa. *Journal of Geophysical Research* **96**, 11831–11848.

Mole, D. R. *et al.* (2014). Archean komatiite volcanism controlled by the evolution of early continents. *Proceedings of the National Academy of Sciences* **111**, 10083–10088.

Mole, D. R., Thurston, P. C., Marsh, J. H., Stern, R. A., Ayer, J. A., Martin, L. A. J. & Lu, Y. J. (2021). The formation of Neoarchean continental crust in the south-east Superior Craton by two distinct geodynamic processes. *Precambrian Research* **356**.

Myhill, R., Frost, D. J. & Novella, D. (2017). Hydrous melting and partitioning in and above the mantle transition zone: Insights from water-rich MgO–SiO2–H2O experiments. *Geochimica et Cosmochimica Acta*. Elsevier Ltd **200**, 408–421.

Nesbitt, R. W. (1971). Skeletal crystal forms in the ultramafic rocks of the Yilgarn Block, Western Australia: evidence for an Archaean ultramafic liquid. *Geological Society of Australia Special Publications* **3**, 331–347.

Nesbitt, R. W., Jahn, B. M. & Purvis, A. C. (1982). Komatiites: An early precambrian phenomenon. *Journal of Volcanology and Geothermal Research* **14**, 31–45.

Nesbitt, R. W., Sun, S.-S. & Purvis, A. C. (1979). Komatiites: Geochemistry and Genesis. *Canadian Mineralogist* **17**, 165–169.

Nicklas, R. W., Puchtel, I. S. & Ash, R. D. (2018). Redox state of the Archean mantle: Evidence from V partitioning in 3.5–2.4 Ga komatiites. *Geochimica et Cosmochimica Acta*. Elsevier Ltd **222**, 447–466.

Nicklas, R. W., Puchtel, I. S., Ash, R. D., Piccoli, P. M., Hanski, E., Nisbet, E. G., Waterton, P., Pearson, D. G. &

Anbar, A. D. (2019). Secular mantle oxidation across the Archean-Proterozoic boundary: Evidence from V partitioning in komatiites and picrites. *Geochimica et Cosmochimica Acta*. Elsevier Ltd **250**, 49–75.

Nisbet, E. G. (1982). The tectonic setting and petrogenesis of komatiites. In: Arndt, N. T. & Nisbet, E. G. (eds) *Komatiites*. London: George Allen & Unwin, 501–520.

Nisbet, E. G., Cheadle, M. J., Arndt, N. T. & Bickle, M. J. (1993). Constraining the potential temperature of the Archaean mantle: A review of the evidence from komatiites. *Lithos* **30**, 291–307.

Nutman, A. P., McGregor, V. R., Friend, C. R. L., Bennett, V. C. & Kinny, P. D. (1996). The Itsaq Gneiss Complex of southern West Greenland; the world's most extensive record of early crustal evolution (3900-3600 Ma). *Precambrian Research* **78**, 1–39.

O'Neill, H. S. C., McCammon, C. A., Canil, D., Rubie, D. C., Ross, C. R. & Seifert, F. (1993). Mossbauer spectroscopy of mantle transition zone phases and determination of minimum Fe3+ content. *American Mineralogist* **78**, 456–460.

Ohtani, E. (1990). Majorite fractionation and genesis of komatiites in the deep mantle. *Precambrian Research* **48**, 195–202.

Ohtani, E., Nagata, Y., Suzuki, A. & Kato, T. (1995). Melting relations of peridotite and the density crossover in planetary mantles. *Chemical Geology* **120**, 207–221.

Ohtani, E. & Suzuki, A. (1996). Density and viscosity of ultramafic magmas at very high pressure: Implications for fractionation in the Earth's mantle. *Misasa seminar on evolutionary processes of Earth and planetary materials*.

Parman, S. W., Dann, J. C., Grove, T. L. & de Wit, M. J. (1997). Emplacement conditions of komatiite magmas from the 3.49 Ga Komati Formation, Barberton Greenstone Belt, South Africa. *Earth and Planetary Science Letters* **150**, 303–323.

Parman, S. W. & Grove, T. L. (2005). Komatiites in the Plume Debate. *Geological Society Of America Special Papers* **388**, 249–256.

Parman, S. W., Grove, T. L., Dann, J. C. & de Wit, M. J. (2004). A subduction origin for komatiites and cratonic lithospheric mantle. *South African Journal of Geology* **107**, 107–118.

Pearce, J. A. & Reagan, M. K. (2019). Identification, classification, and interpretation of boninites from Anthropocene to Eoarchean using Si-Mg-Ti systematics. *Geosphere* **15**, 1008–1037.

Pearson, D. G. *et al.* (2014). Hydrous mantle transition zone indicated by ringwoodite included within diamond. *Nature*. Nature Publishing Group **507**, 221–224.

Pearson, D. G., Carlson, R. W., Shirey, S. B., Boyd, F. R. & Nixon, P. H. (1995). Stabilisation of Archaean lithospheric mantle: A Re–Os isotope study of peridotite xenoliths from the Kaapvaal craton. *Earth and Planetary Science Letters* **134**, 341–357.

Pierru, R., Andrault, D., Manthilake, G., Monteux, J., Devidal, J. L., Guignot, N., King, A. & Henry, L. (2022). Deep mantle origin of large igneous provinces and komatiites. *Science advances* **8**, eabo1036.

Plank, T. & Langmuir, C. H. (1992). Effects of the Melting Regime on the Composition of the Oceanic Crust. *Journal of Geophysical Research* **97**, 19749–19770.

Puchtel, I. S., Blichert-Toft, J., Horan, M. F., Touboul, M. & Walker, R. J. (2022). The komatiite testimony to ancient mantle heterogeneity. *Chemical Geology*. Elsevier B.V. **594**.

Puchtel, I. S., Blichert-Toft, J., Touboul, M., Horan, M. F. & Walker, R. J. (2016). The coupled 182W-142Nd record of early terrestrial mantle differentiation. *Geochemistry Geophysics Geosystems* **17**, 2168–2193.

Puchtel, I. S., Blichert-Toft, J., Touboul, M. & Walker, R. J. (2018). 182W and HSE constraints from 2.7 Ga komatiites on the heterogeneous nature of the Archean mantle. *Geochimica et Cosmochimica Acta* **228**, 1–26.

Puchtel, I. S., Blichert-Toft, J., Touboul, M., Walker, R. J., Byerly, G. R., Nisbet, E. G. & Anhaeusser, C. R. (2013). Insights into early Earth from Barberton komatiites: Evidence from lithophile isotope and trace element systematics. *Geochimica et Cosmochimica Acta*. Elsevier Ltd **108**, 63–90.

Puchtel, I. S., Haase, K. M., Hofmann, A. W., Chauvel, C., Kulikov, V. S., Garbe-Schönberg, C. D. & Nemchin, A. A. (1997). Petrology and geochemistry of crustally contaminated komatiitic basalts from the Vetreny Belt, southeastern Baltic Shield: Evidence for an early Proterozoic mantle plume beneath rifted Archean continental lithosphere. *Geochimica et Cosmochimica Acta* **61**, 1205–1222.

Puchtel, I. S., Hofmann, A. W., Mezger, K., Jochum, K. P., Shchipansky, A. A. & Samsonov, A. V. (1998). Oceanic plateau model for continental crustal growth in the Archaean: A case study from the Kostomuksha greenstone belt, NW Baltic Shield. *Earth and Planetary Science Letters* **155**, 57–74.

Puchtel, I. S., Hofmann, A. W., Mezger, K., Shchipansky, A. A., Kulikov, V. S. & Kulikova, V. V. (1996). Petrology of a 2.41 Ga remarkably fresh komatiitic basalt lava lake in Lion Hills, central Vetreny Belt, Baltic Shield. *Contributions to Mineralogy and Petrology* **124**, 273–290.

Puchtel, I. S., Humayun, M., Campbell, A. J., Sproule, R. A. & Lesher, C. M. (2004). Platinum group element geochemistry of komatiites from the Alexo and Pyke Hill areas, Ontario, Canada. *Geochimica et Cosmochimica Acta* **68**, 1361–1383.

Puchtel, I. S., Mundl-Petermeier, A., Horan, M., Hanski, E. J., Blichert-Toft, J. & Walker, R. J. (2020). Ultra-depleted 2.05 Ga komatiites of Finnish Lapland: Products of grainy late accretion or core-mantle interaction? *Chemical Geology*. Elsevier **554**.

Puetz, S. J. & Condie, K. C. (2019). Time series analysis of mantle cycles Part I: Periodicities and correlations among seven global isotopic databases. *Geoscience Frontiers*. Elsevier Ltd **10**, 1305–1326.

Pyke, D. R., Naldrett, A. J. & Eckstrand, O. R. (1973). Archean ultramafic flows in Munro Township, Ontario. *Bulletin of the Geological Society of America* **84**, 955–978.

Renner, R., Nisbet, E. G., Cheadle, M. J., Arndt, N. T., Bickle, M. J. & Cameron, W. E. (1994). Komatiite flows from the reliance formation, belingwe belt, Zimbabwe: I. petrography and mineralogy. *Journal of Petrology* **35**, 361–400.

Révillon, S., Arndt, N. T., Chauvel, C. & Hallot, E. (2000). Geochemical Study of Ultramafic Volcanic and Plutonic Rocks from Gorgona Island, Colombia: the Plumbing System of an Oceanic Plateau. *Journal of Petrology* **41**, 1127–1153.

Robin-Popieul, C. C. M., Arndt, N. T., Chauvel, C., Byerly, G. R., Sobolev, A. V. & Wilson, A. (2012). A new model for Barberton komatiites: Deep critical melting with high melt retention. *Journal of Petrology* **53**, 2191–2229.

Roeder, P. L. & Emslie, R. F. (1970). Olivine-liquid equilibrium. *Contributions to Mineralogy and Petrology* **29**, 275–289.

Rohrbach, A., Ballhaus, C., Golla-Schindler, U., Ulmer, P., Kamenetsky, V. S. & Kuzmin, D. V (2007). Metal saturation in the upper mantle. *Nature* **449**, 456–458.

Rohrbach, A., Ballhaus, C., Ulmer, P., Golla-Schindler, U. & Schönbohm, D. (2011). Experimental evidence for a reduced metal-saturated upper mantle. *Journal of Petrology* **52**, 717–731.

Rollinson, H., Appel, P. W. U. & Frei, R. (2002). A Metamorphosed, Early Archaean Chromitite from West Greenland: Implications for the Genesis of Archaean Anorthositic Chromitites. *Journal of Petrology* **43**, 2143–2170.

Rudge, J. F., Maclennan, J. & Stracke, A. (2013). The geochemical consequences of mixing melts from a heterogeneous mantle. *Geochimica et Cosmochimica Acta*. Elsevier Ltd **114**, 112–143.

Salters, V. J. M. & Stracke, A. (2004). Composition of the depleted mantle. *Geochemistry, Geophysics, Geosystems* **5**.

Saverikko, M. (1985). The pyroclastic komatiite complex at Sattasvaara in northern Finland. *Geological Society of Finland, Bulletin* **57**, 55–87.

Schmeling, H. & Arndt, N. (2017). Modelling komatiitic melt accumulation and segregation in the transition zone. *Earth and Planetary Science Letters*. Elsevier B.V. **472**, 95–106.

Serrano, L., Ferrari, L., Martínez, M. L., Petrone, C. M. & Jaramillo, C. (2011). An integrative geologic, geochronologic and geochemical study of Gorgona Island, Colombia: Implications for the formation of the Caribbean Large Igneous Province. *Earth and Planetary Science Letters*. Elsevier B.V. **309**, 324–336.

Shimizu, K., Komiya, T., Hirose, K., Shimizu, N. & Maruyama, S. (2001). Cr-spinel, an excellent micro-container for retaining primitive melts - Implications for a hydrous plume origin for komatiites. *Earth and Planetary Science Letters* **189**, 177–188.

Shore, M. & Fowler, D. (1999). The origin of spinifex texture in komatiites. *Nature* **397**, 691–694.

Siégel, C., Arndt, N., Barnes, S., Henriot, A. L., Haenecour, P., Debaille, V. & Mattielli, N. (2014). Fred's Flow (Canada) and Murphy Well (Australia): thick komatiitic lava flows with contrasting compositions, emplacement mechanisms and water contents. *Contributions to Mineralogy and Petrology* **168**, 1–17.

Smyth, J. R. (1994). A crystallographic model for hydrous wadsleyite (β-Mg2SiO4): An ocean in the Earth's interior? *American Mineralogist* **79**, 1021–1024.

Snoke, A. W. & Calk, L. C. (1978). Jackstraw-textured talc-olivine rocks, Preston Peak area, Klamath Mountains, California. *Bulletin of the Geological Society of America* **89**, 223–230.

Sobolev, A. V., Asafov, E. V., Gurenko, A. A., Arndt, N. T., Batanova, V. G., Portnyagin, M. V., Garbe-Schönberg,

D., Wilson, A. H. & Byerly, G. R. (2019). Deep hydrous mantle reservoir provides evidence for crustal recycling before 3.3 billion years ago. *Nature* **571**, 555–559.

Sobolev, A. V, Asafov, E. V, Gurenko, A. A., Arndt, N. T., Batanova, V. G., Portnyagin, M. V, Garbe-Schönberg, D. & Krasheninnikov, S. P. (2016). Komatiites reveal a hydrous Archaean deep-mantle reservoir. *Nature*. Nature Publishing Group **531**, 628–632.

Sobolev, A. V & Chaussidon, M. (1996). H2O concentrations in primary melts from supra-subduction zones and mid-ocean ridges: Implications for H2O storage and recycling in the mantle. *Earth and Planetary Science Letters* **137**, 45–55.

Sossi, P. A., Eggins, S. M., Nesbitt, R. W., Nebel, O., Hergt, J. M., Campbell, I. H., O'Neill, H. S. C., Kranendonk, M. Van & Rhodri Davies, D. (2016). Petrogenesis and geochemistry of Archean Komatiites. *Journal of Petrology* **57**, 147–184.

Sproule, R. A., Lesher, C. M., Ayer, J. A., Thurston, P. C. & Herzberg, C. T. (2002). Spatial and temporal variations in the geochemistry of komatiites and komatiitic basalts in the Abitibi greenstone belt. *Precambrian Research* **115**, 153–186.

Stolper, E., Walker, D., Hager, B. H. & Hays, J. F. (1981). Melt Segregation From Partially Molten Source Regions: The Importance of Melt Density and Source Region Size. *Journal of Geophysical Research* **86**, 6261–6271.

Stone, W. E., Crocket, J. H., Dickin, A. P. & Fleet, M. E. (1995). Origin of Archean ferropicrites: geochemical constraints from the Boston Creek Flow, Abitibi greenstone belt, Ontario, Canada. *Chemical Geology* **121**, 51–71.

Stone, W. E., Deloule, E., Larson, M. S. & Lesher, C. M. (1997). Evidence for hydrous high-MgO melts in the Precambrian. *Geology* **25**, 143–146.

Stracke, A., Genske, F., Berndt, J. & Koornneef, J. M. (2019). Ubiquitous ultra-depleted domains in Earth's mantle. *Nature Geoscience*. Springer US **12**, 851–855.

Szilas, K., van Hinsberg, V., McDonald, I., Næraa, T., Rollinson, H., Adetunji, J. & Bird, D. (2018). Highly refractory Archaean peridotite cumulates: Petrology and geochemistry of the Seqi Ultramafic Complex, SW Greenland. *Geoscience Frontiers*. Elsevier Ltd **9**, 689–714.

Thurston, P. C., Ayer, J. A., Goutier, J. & Hamilton, M. A. (2008). Depositional gaps in abitibi greenstone belt stratigraphy: A key to exploration for syngenetic mineralization. *Economic Geology* **103**, 1097–1134.

Timmerman, S. *et al.* (2022). Mesoarchean diamonds formed in thickened lithosphere, caused by slab-stacking. *Earth and Planetary Science Letters*. Elsevier B.V. **592**, 117633.

Tomlinson, E. L. & Holland, T. J. B. (2021). A Thermodynamic Model for the Subsolidus Evolution and Melting of Peridotite. *Journal of Petrology* **62**, 1–23.

Tomlinson, E. L. & Kamber, B. S. (2021). Depth-dependent peridotite-melt interaction and the origin of variable silica in the cratonic mantle. *Nature Communications*. Springer US **12**, 1–15.

Toplis, M. J. (2005). The thermodynamics of iron and magnesium partitioning between olivine and liquid: Criteria for assessing and predicting equilibrium in natural and experimental systems. *Contributions to Mineralogy and Petrology* **149**, 22–39.

Trela, J., Gazel, E., Sobolev, A. V, Moore, L., Bizimis, M., Jicha, B. & Batanova, V. G. (2017). The hottest lavas of the Phanerozoic and the survival of deep Archaean reservoirs. *Nature Geosci* **10**, 451–456.

Turner, J. S., Huppert, H. E. & Sparks, R. S. J. (1986). Komatiites II: Experimental and Theoretical Investigations of Post-emplacement Cooling and Crystallization. *Journal of Petrology* **27**, 397–437.

Van Kranendonk, M. J., Hugh Smithies, R., Hickman, A. H. & Champion, D. C. (2007). Review: Secular tectonic evolution of Archean continental crust: interplay between horizontal and vertical processes in the formation of the Pilbara Craton, Australia. *Terra Nova* **19**, 1–38.

Viljoen, M. J. & Viljoen, R. P. (1969). The geology and geochemistry of the lower ultramafic unit of the Onverwacht group and a proposed new class of igneous rocks. *Geological Survey of South Africa, Special Publication* **21**, 55–85.

Walsh, C., Kamber, B. S. & Tomlinson, E. L. (2023). Deep, ultra-hot-melting residues as cradles of mantle diamond. *Nature*. Springer US **615**, 450–454.

Walter, M. J. (1998). Melting of garnet peridotite and the origin of komatiite and depleted lithosphere. *Journal of Petrology* **39**, 29–60.

Wan, Z., Coogan, L. a. & Canil, D. (2008). Experimental calibration of aluminum partitioning between olivine and spinel as a geothermometer. *American Mineralogist* **93**, 1142–1147.

Waterton, P., Mungall, J. & Pearson, D. G. (2021). The komatiite-mantle platinum-group element paradox. *Geochimica et Cosmochimica Acta*. The Author(s) **313**, 214–242.

Waterton, P., Pearson, D. G., Kjarsgaard, B., Hulbert, L., Locock, A., Parman, S. W. & Davis, B. (2017). Age, Origin, and Thermal Evolution of the ultra-fresh ~1.9 Ga Winnipegosis Komatiites, Manitoba, Canada. *Lithos*. Elsevier B.V. **268**–**271**, 114–130.

Waterton, P., Pearson, D. G., Mertzman, S. A., Mertzman, K. R. & Kjarsgaard, B. A. (2020). A Fractional Crystallization Link between Komatiites, Basalts, and Dunites of the Palaeoproterozoic Winnipegosis Komatiite Belt, Manitoba, Canada. *Journal of Petrology* **61**, egaa052, 1–34.

Wilson, A. & Bolhar, R. (2022). Olivine in komatiite records origin and travel from the deep upper mantle. *Geology* **50**, 351–355.

Wilson, A. H. (2019). The Late-Paleoarchean Ultra-Depleted Commondale Komatiites: Earth's Hottest Lavas and Consequences for Eruption. *Journal of Petrology* **60**, 1575–1620.

Wilson, A. H., Shirey, S. B. & Carlson, R. W. (2003). Archaean ultra-depleted komatiites formed by hydrous melting of cratonic mantle. *Nature* **423**, 858–861.

Wilson, A. & Riganti, A. (2022). Architectural and Compositional Diversity of Early Earth Ocean Floor Evidenced by the Paleoarchean Nondweni Greenstone Belt, South Africa. *Journal of Petrology* **63**, 1–32.

Wyman, D. (2020). Komatiites From Mantle Transition Zone Plumes. *Frontiers in Earth Science* **8**.

Xie, L., Yoneda, A., Katsura, T., Andrault, D., Tange, Y. & Higo, Y. (2021). Direct Viscosity Measurement of Peridotite Melt to Lower-Mantle Conditions: A Further Support for a Fractional Magma-Ocean Solidification at the Top of the Lower Mantle. *Geophysical Research Letters* **48**, 1–8.

Yoshino, T., Nishihara, Y. & Karato, S. ichiro (2007). Complete wetting of olivine grain boundaries by a hydrous melt near the mantle transition zone. *Earth and Planetary Science Letters* **256**, 466–472.

Figure 1

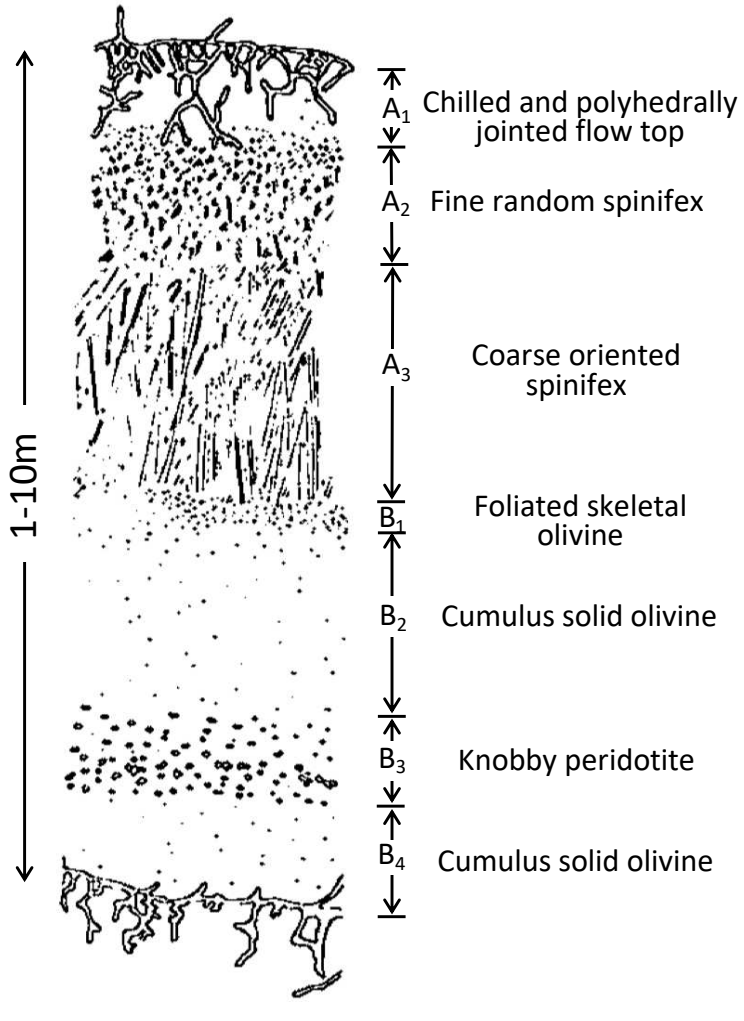

A. Spinifex-textured flow

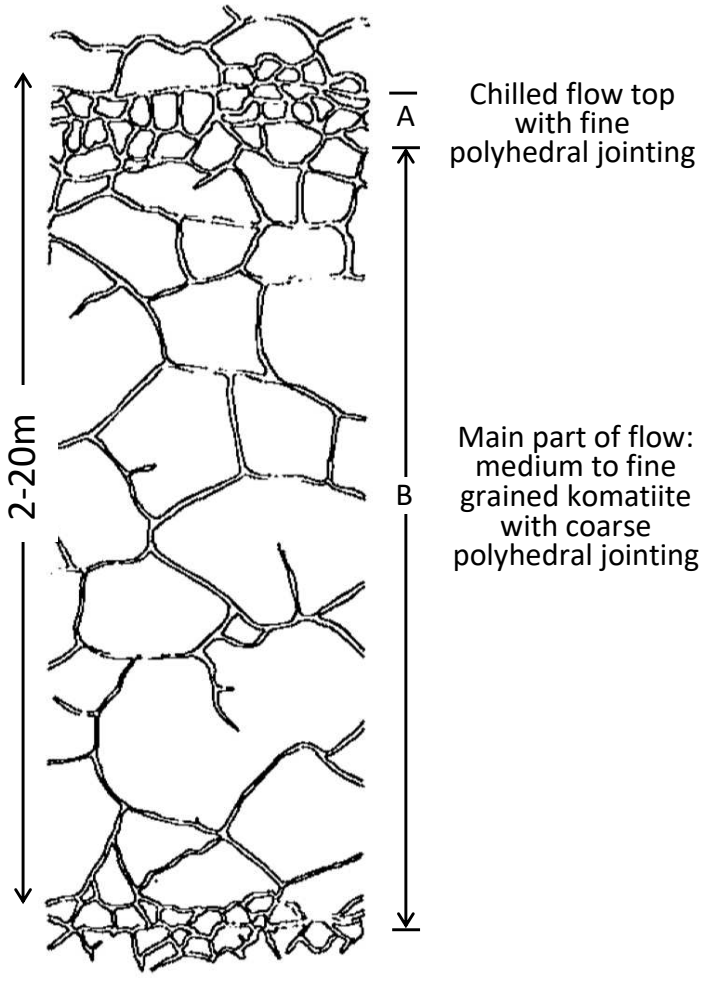

B. Massive flow

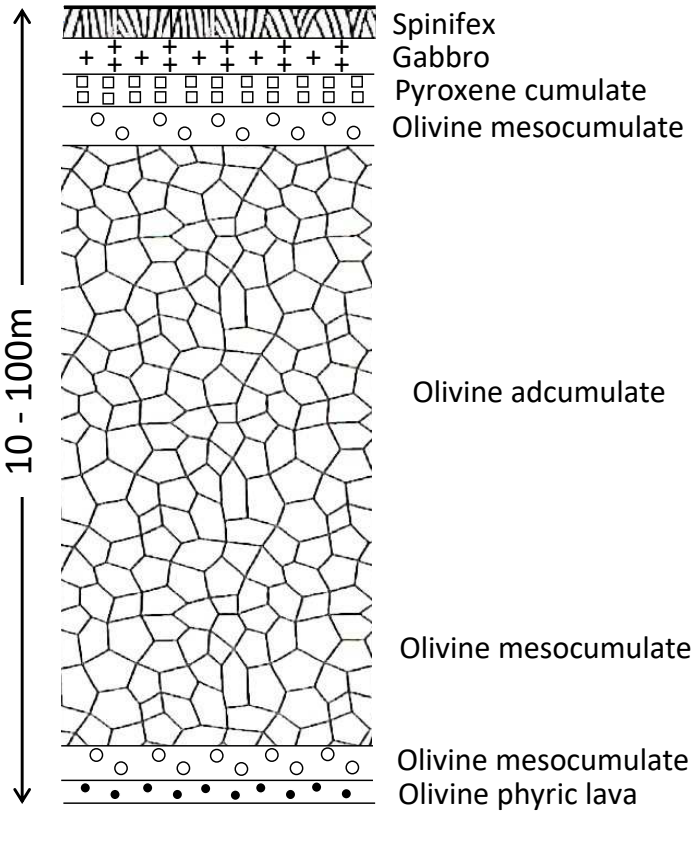

C. Thick cumulate-dominated flow

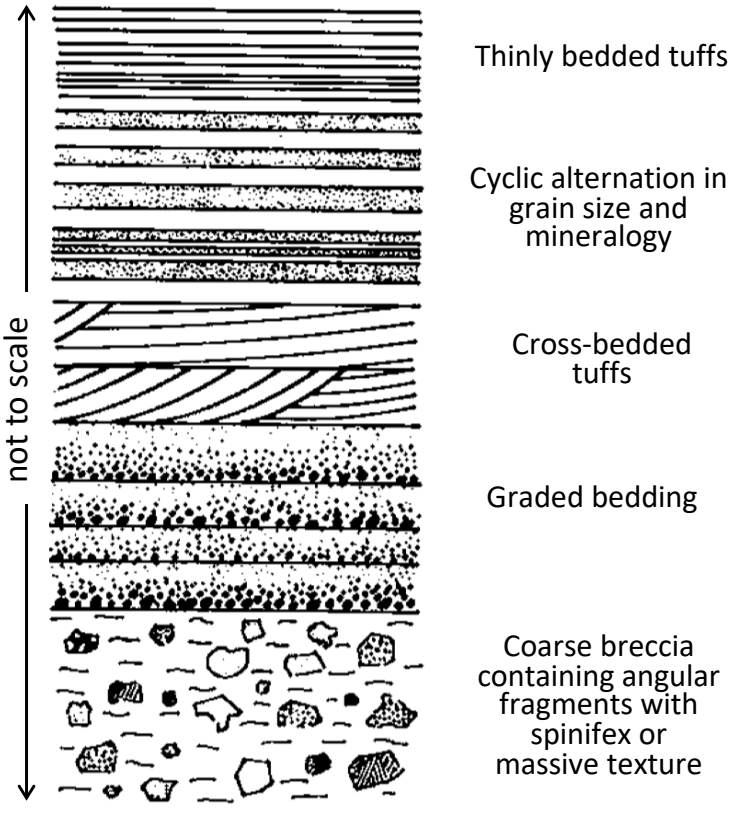

D. Volcanoclastic

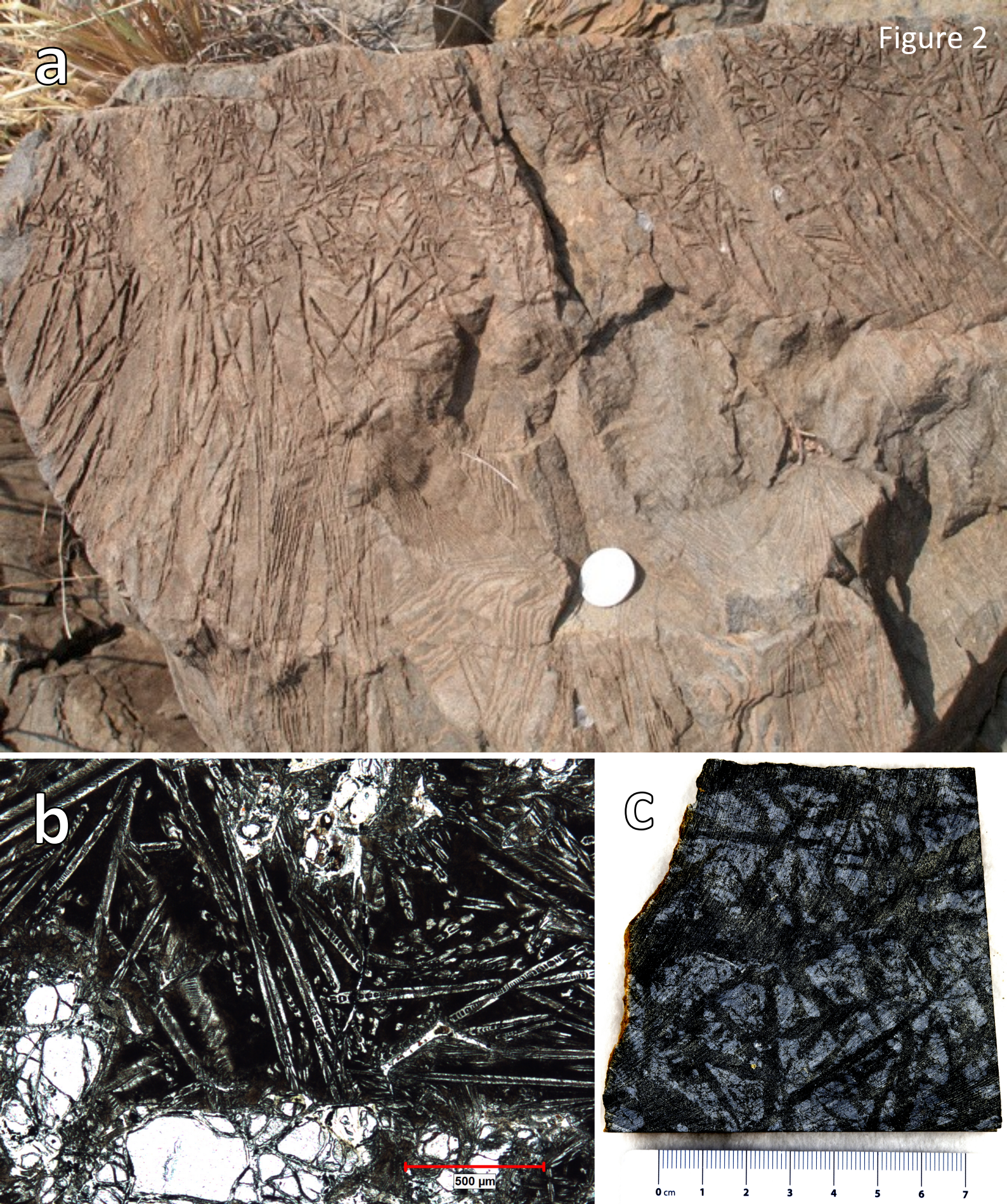
Figure 2
a
b
500 µm
c
0 cm
1
2
3
4
5
6
7

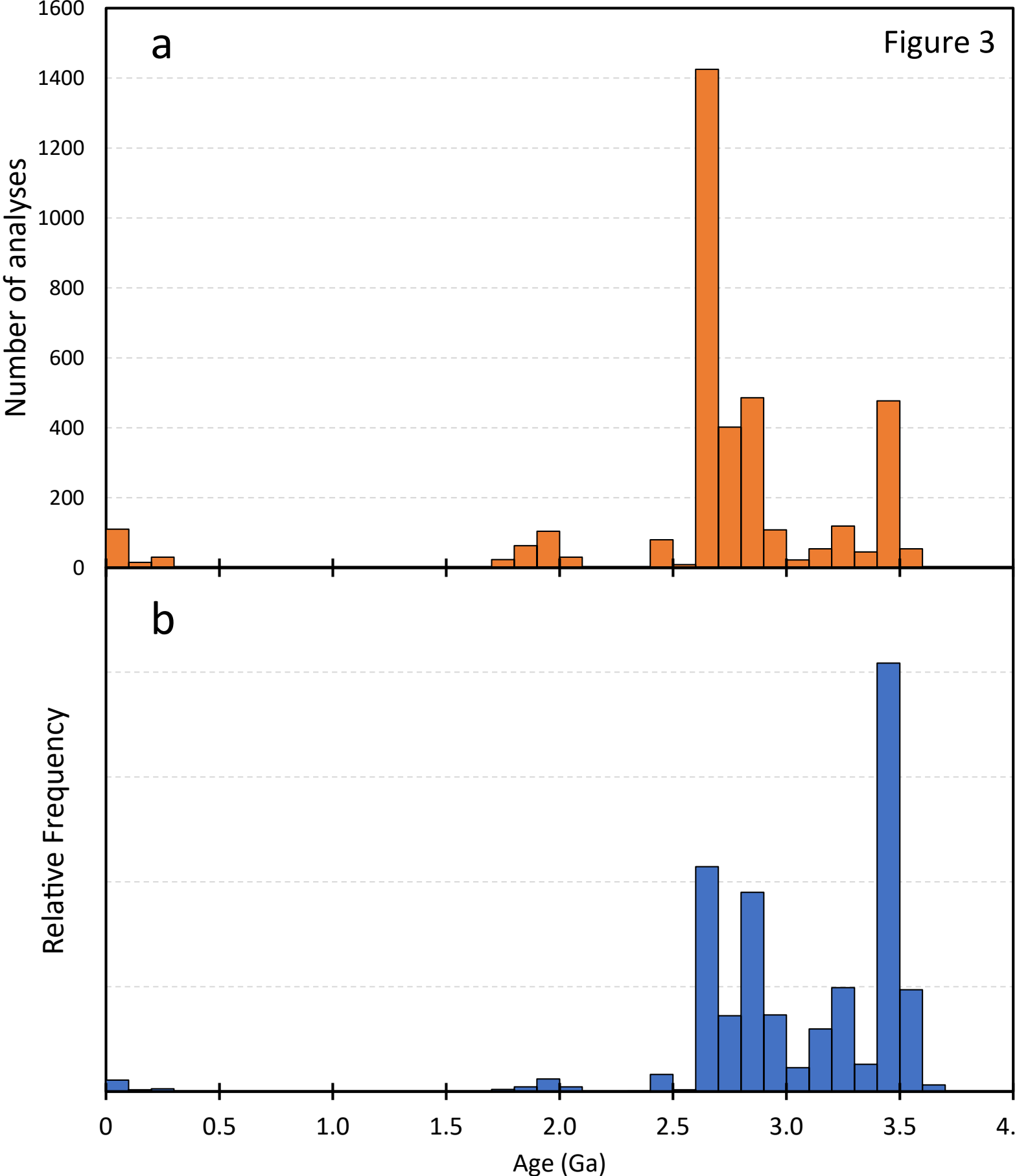
a
Figure 3
Number of analyses
1600
1400
1200
1000
800
600
400
200
0
b
Relative Frequency
0
0.5
1.0
1.5
2.0
2.5
3.0
3.5
4.0
Age (Ga)

Figure 4

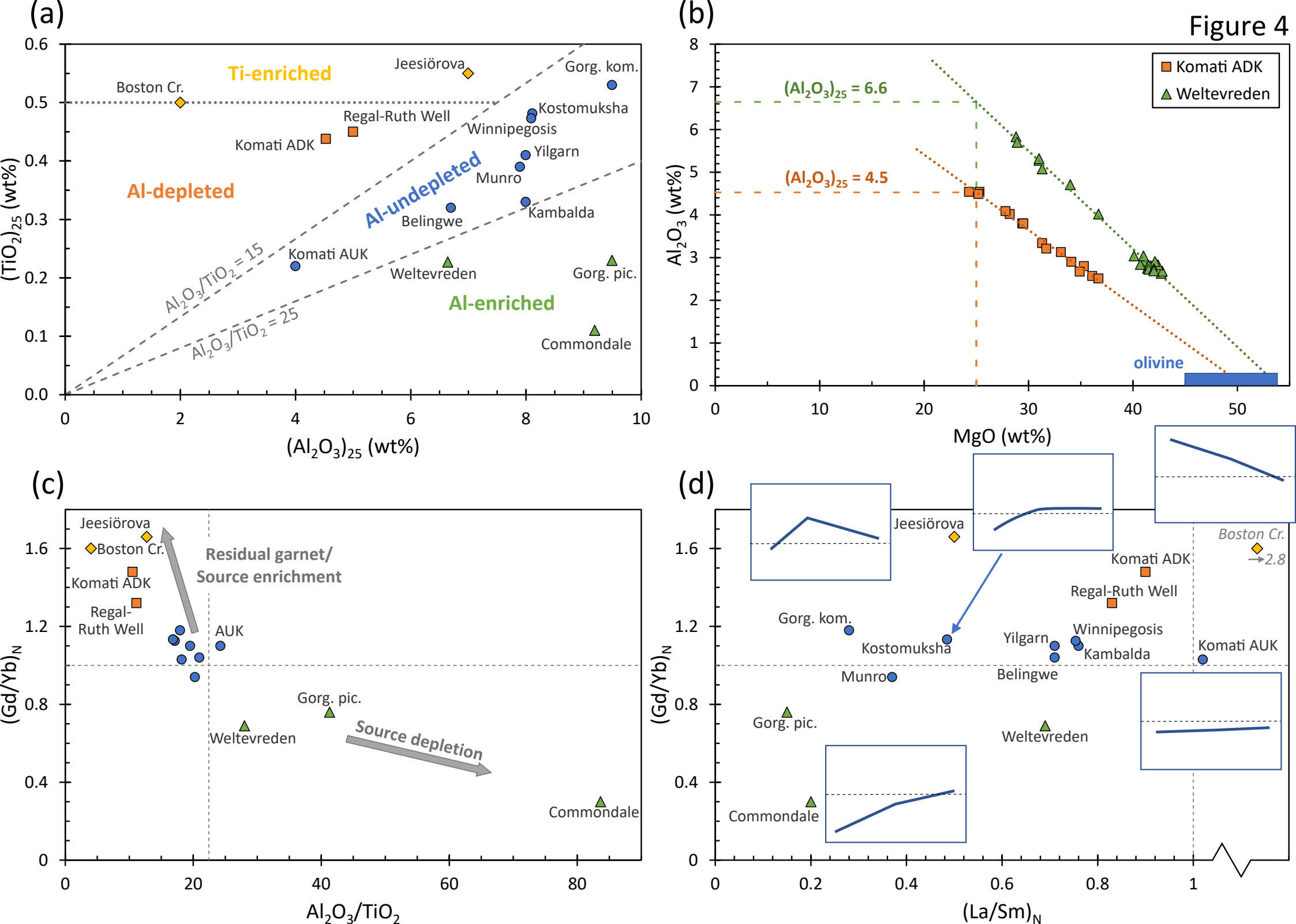
(a)
Ti-enriched
Al-depleted
Al-undepleted
Al-enriched
Boston Cr.
Jeesiörova
Gorg. kom.
Regal-Ruth Well
Kostomuksha
Winnipegosis
Komati ADK
Yilgarn
Munro
Belingwe
Kambalda
Komati AUK
Weltevreden
Gorg. pic.
Commondale
Al2O3/TiO2 = 15
Al2O3/TiO2 = 25
(TiO2)25 (wt%)
(Al2O3)25 (wt%)
(b)
(Al2O3)25 = 6.6
(Al2O3)25 = 4.5
Komati ADK
Weltevreden
olivine
Al2O3 (wt%)
MgO (wt%)
(c)
Residual garnet/
Source enrichment
Source depletion
(Gd/Yb)N
Al2O3/TiO2
(d)
Boston Cr.
2.8
(La/Sm)N

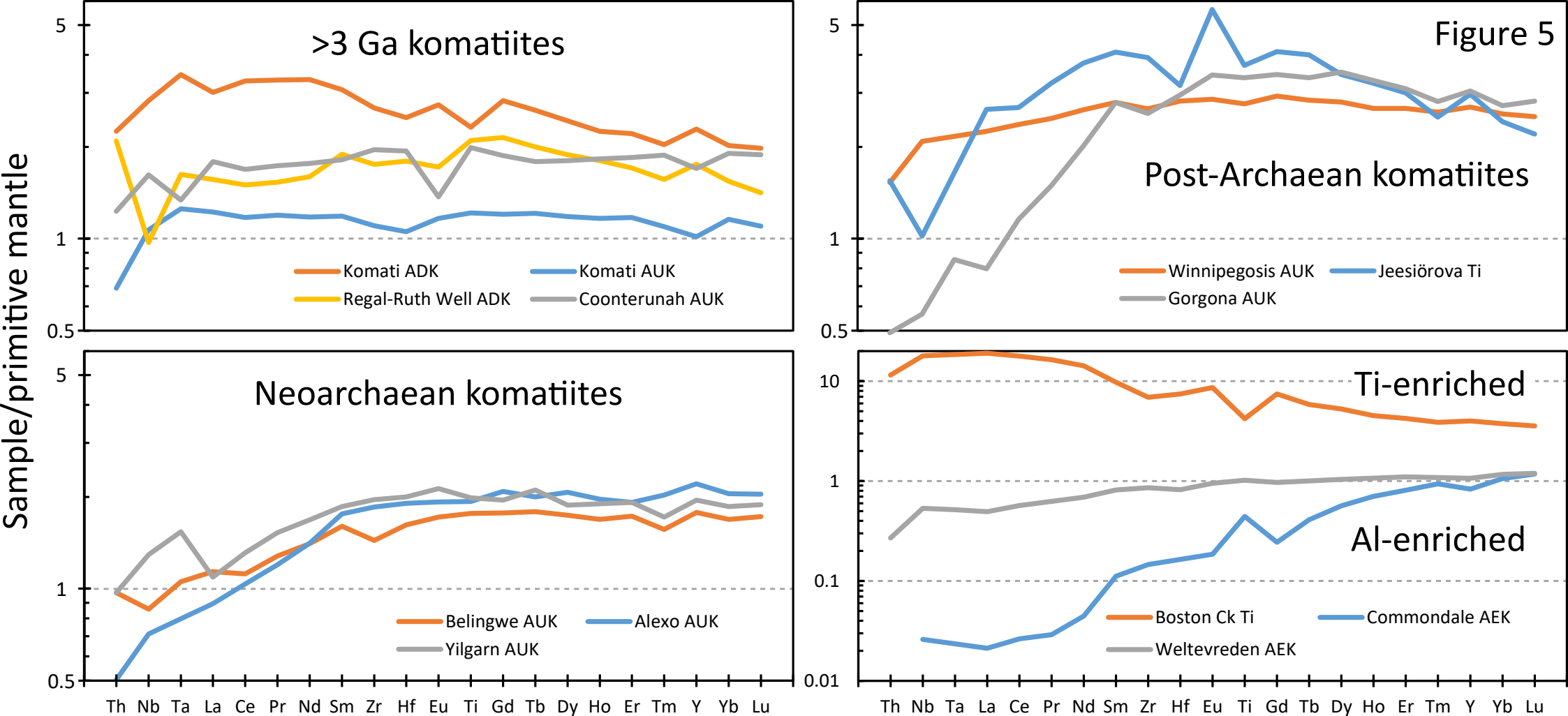
Figure 5
>3 Ga komatiites
Komati ADK
Komati AUK
Regal-Ruth Well ADK
Coonterunah AUK
Post-Archaean komatiites
Winnipegosis AUK
Jeesiörova Ti
Gorgona AUK
Neoarchaean komatiites
Belingwe AUK
Alexo AUK
Yilgarn AUK
Ti-enriched
Al-enriched
Boston Ck Ti
Commondale AEK
Weltevreden AEK
Sample/primitive mantle
5
1
0.5
10
0.1
0.01
Th Nb Ta La Ce Pr Nd Sm Zr Hf Eu Ti Gd Tb Dy Ho Er Tm Y Yb Lu

Figure 6

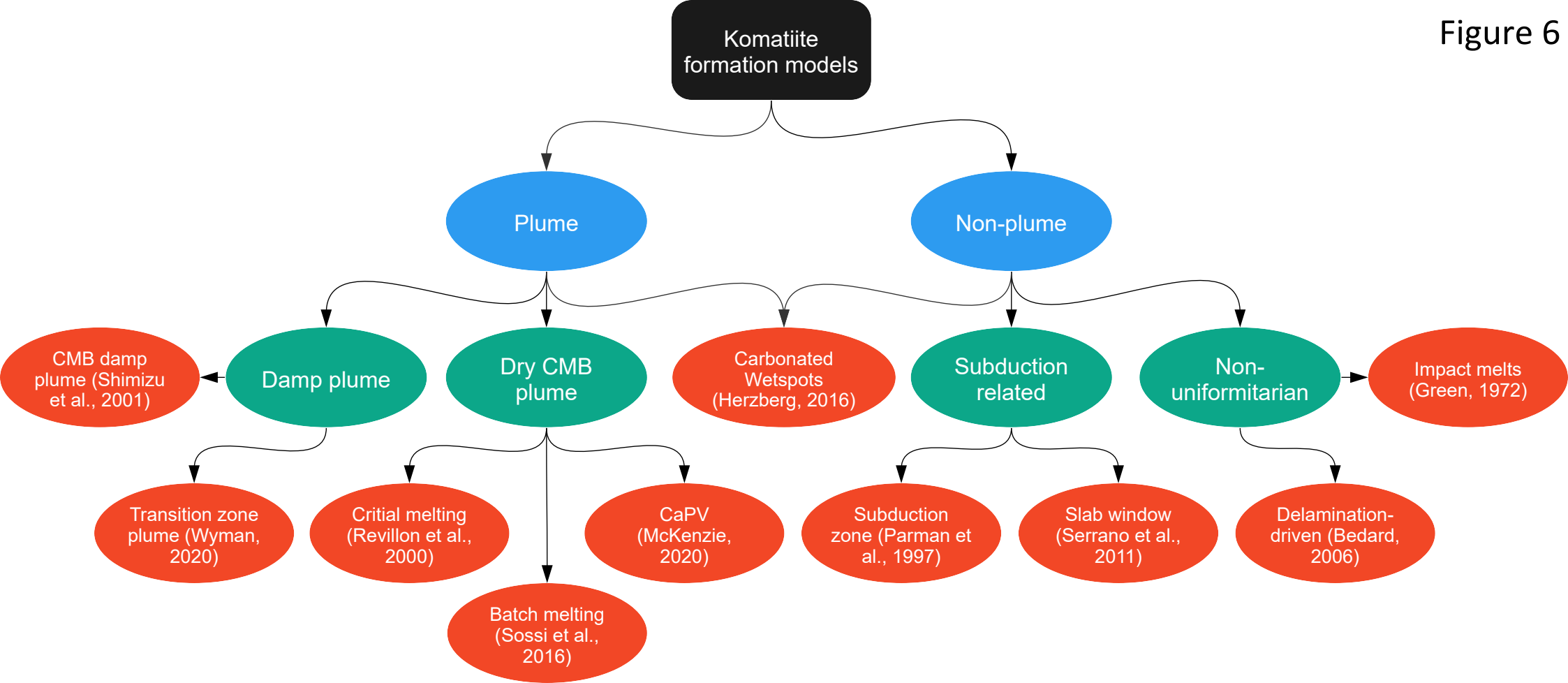
Komatiite formation models
Plume
Non-plume
CMB damp plume (Shimizu et al., 2001)
Damp plume
Dry CMB plume
Carbonated Wetspots (Herzberg, 2016)
Subduction related
Non-uniformitarian
Impact melts (Green, 1972)
Transition zone plume (Wyman, 2020)
Critial melting (Revillon et al., 2000)
CaPV (McKenzie, 2020)
Batch melting (Sossi et al., 2016)
Subduction zone (Parman et al., 1997)
Slab window (Serrano et al., 2011)
Delamination-driven (Bedard, 2006)

Figure 7

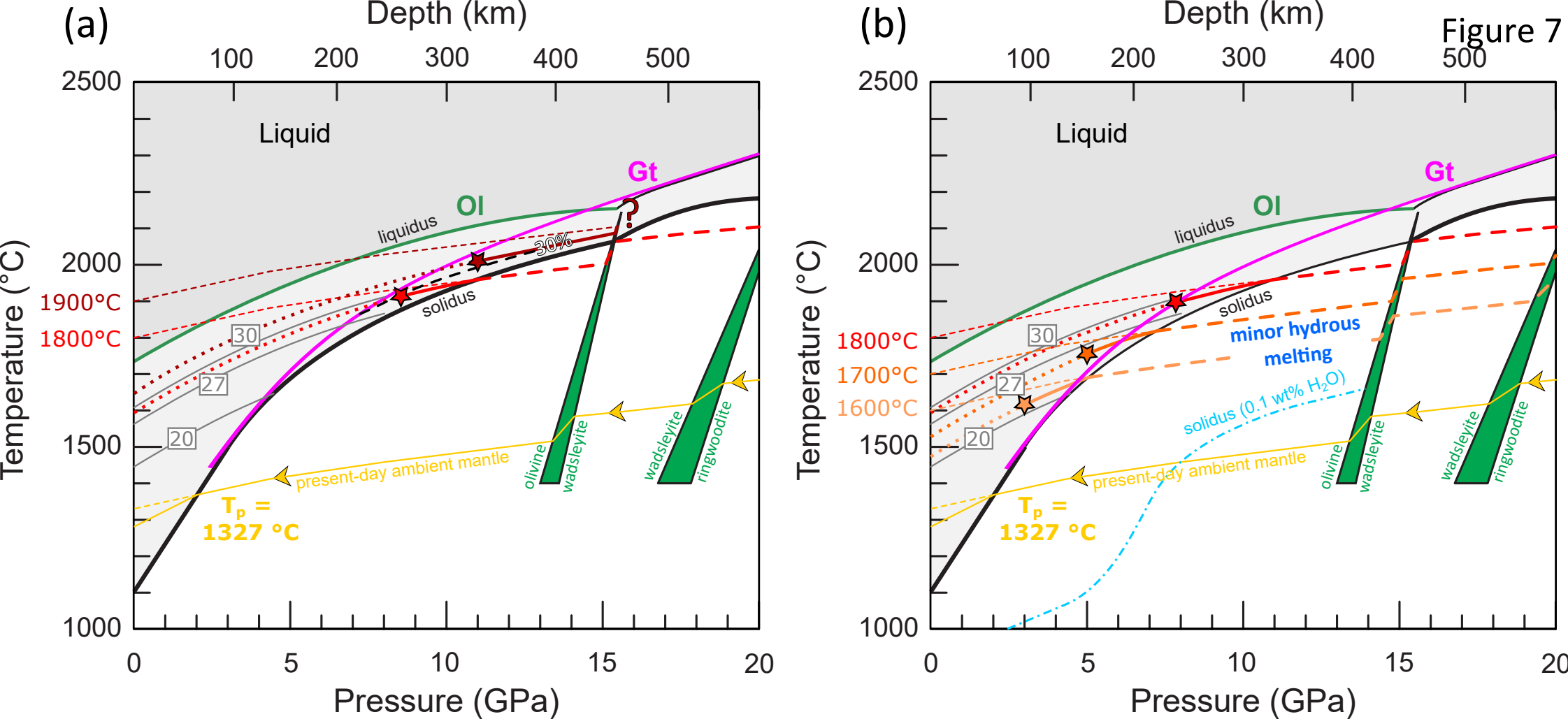
(a)
Depth (km)
100
200
300
400
500
2500
2000
1900°C
1800°C
1500
1000
Temperature (°C)
Liquid
Gt
Ol
liquidus
30%
solidus
30
27
20
present-day ambient mantle
olivine
wadsleyite
wadsleyite
ringwoodite
T_p =
1327 °C
0
5
10
15
20
Pressure (GPa)
(b)
Depth (km)
100
200
300
400
500
2500
2000
1800°C
1700°C
1600°C
1500
1000
Temperature (°C)
Liquid
Gt
Ol
liquidus
solidus
minor hydrous
melting
solidus (0.1 wt% H_2O)
30
27
20
present-day ambient mantle
olivine
wadsleyite
wadsleyite
ringwoodite
T_p =
1327 °C
0
5
10
15
20
Pressure (GPa)

Figure 8

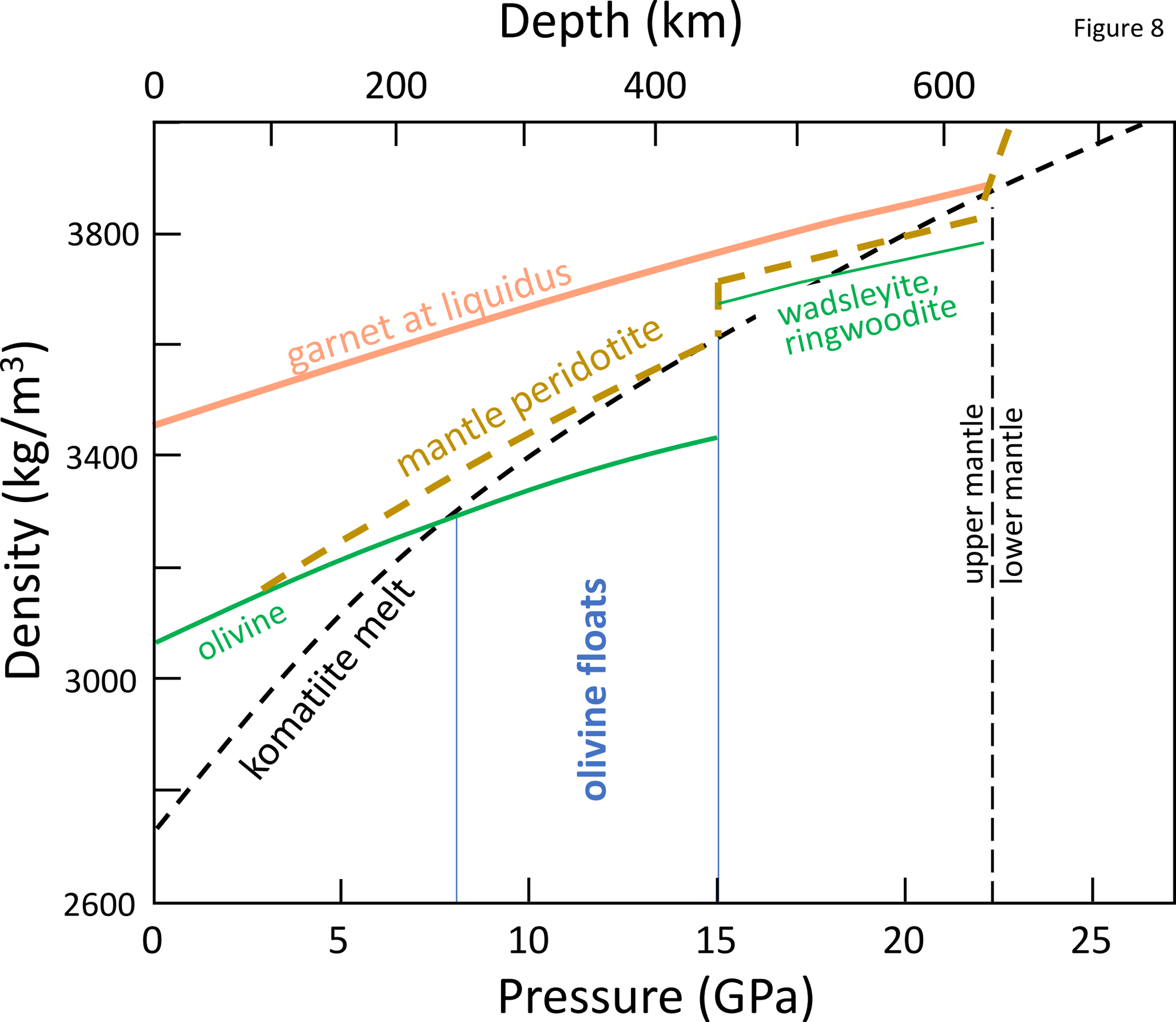
Depth (km)
0
200
400
600
3800
3400
3000
2600
Density (kg/m3)
garnet at liquidus
mantle peridotite
wadsleyite,
ringwoodite
olivine
komatiite melt
olivine floats
upper mantle
lower mantle
0
5
10
15
20
25
Pressure (GPa)

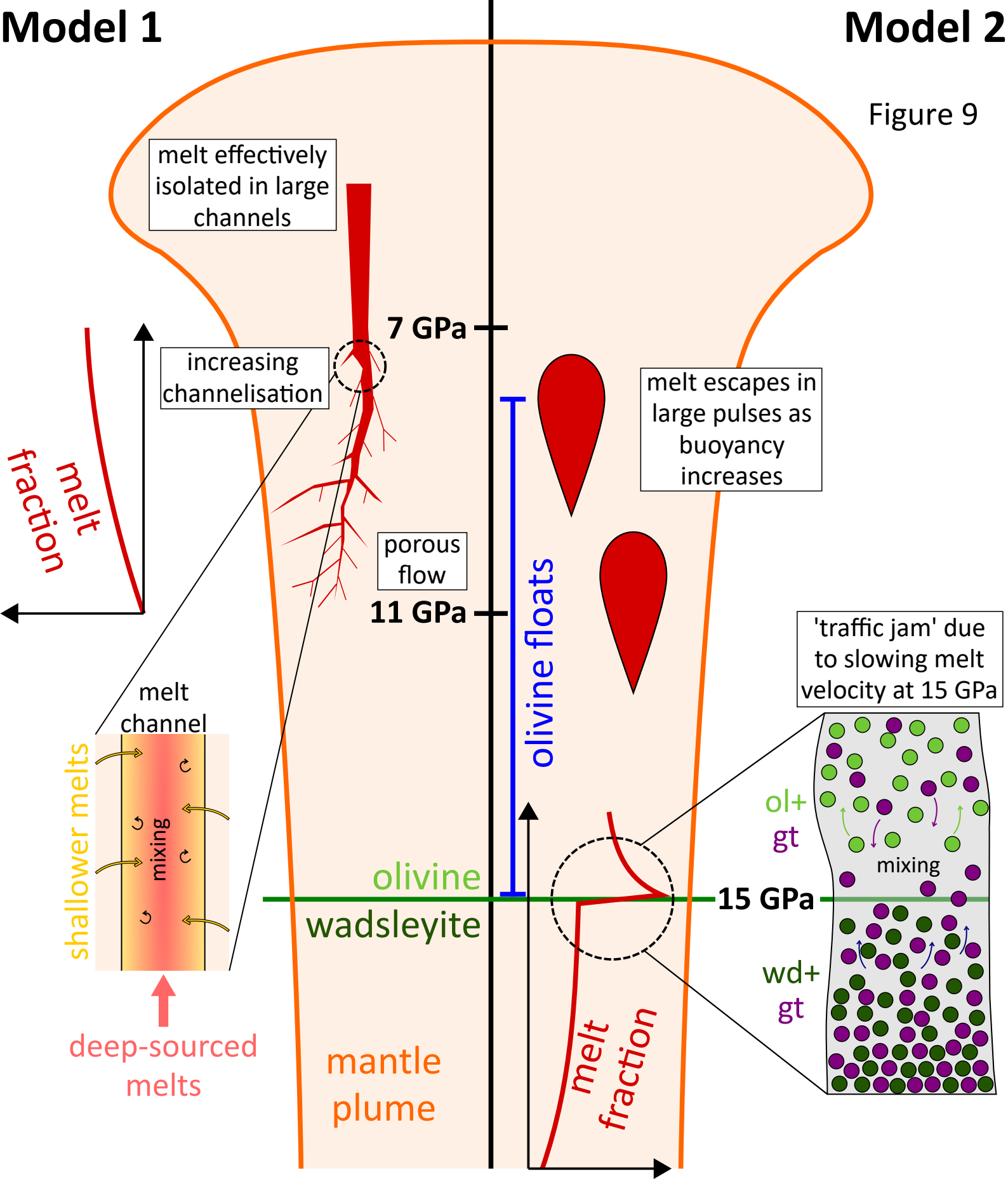
Model 1
Model 2
Figure 9
melt effectively isolated in large channels
7 GPa
increasing channelisation
melt fraction
melt escapes in large pulses as buoyancy increases
porous flow
11 GPa
olivine floats
'traffic jam' due to slowing melt velocity at 15 GPa
melt channel
shallower melts
mixing
ol+ gt
mixing
olivine
15 GPa
wadsleyite
wd+ gt
deep-sourced melts
mantle plume
melt fraction